Undecaprenyl Pyrophosphate Phosphatase (UppP) is a pivotal element in *Salmonella* Intramacrophage Survival

Rhea Vij[1], Debapriya Mukherjee[1#], Kirti Parmar[1#], Krishna Chaitanya Nallamotu[2,3], Manjula Reddy[2,3], Dipshikha Chakravortty[1,4*]

[1]Department of Microbiology and Cell Biology, Indian Institute of Science, Bangalore 560012, India.

[2]CSIR-Centre for Cellular and Molecular Biology, Hyderabad, Telangana 500007, India

[3]Academy of Scientific and Innovative Research (AcSIR), Ghaziabad, Uttar Pradesh, India

[4]Adjunct Faculty, Indian Institute of Science Research and Education, Thiruvananthapuram, Kerala, India

[#]Equal contribution

[*]Corresponding author: dipa@iisc.ac.in

Tel: 0091 80 2293 2842

Fax: 0091 80 2360 2697

Abstract

To establish infection, *Salmonella* confronts a dynamic barrage of host-induced stresses. The peptidoglycan layer, essential for maintaining cell integrity and counteracting environmental stress, relies on the lipid carrier undecaprenyl phosphate, generated by Undecaprenyl pyrophosphate phosphatase (UppP). While UppP is linked to virulence in other pathogens, its role in *Salmonella* remains unclear. We show that an *uppP* mutant in *S*. Typhimurium exhibits

altered cell morphology, reduced stiffness, and impaired survival in RAW 264.7 macrophages. The mutant is also attenuated in systemic infection in C57BL/6 mice. These defects are associated with increased sensitivity to nitrosative stress. Notably, iNOS inhibition or deficiency restores intracellular survival of the *uppP* mutant in both RAW 264.7 macrophages and the mouse model, implicating UppP in resistance to nitrosative stress. Our findings reveal a critical role for UppP in promoting *Salmonella* survival within macrophages and contributing to systemic pathogenesis.

Introduction

Salmonella is a Gram-negative foodborne pathogen belonging to the *Enterobacteriaceae* family [1]. The genus, comprising more than 2600 serovars, can infect various hosts, including plants, birds, and mammals[2], [3]. Clinical manifestations of *Salmonella* infection range from self-limiting gastroenteritis associated with non-typhoidal serovars to systemic infection caused by typhoidal serovars and invasive non-typhoidal serovars [4]. The significant burden of *Salmonella*-associated enterocolitis, affecting 95.1 million people in 2017, coupled with the rising threat of drug-resistant strains as recognised by its inclusion on the WHO priority pathogen list, underscores *Salmonella*'s growing danger to public health [5], [6], [7].

Salmonella enters the host through contaminated food and water. *Salmonella* encounters several stresses within the host, including oxidative and nitrosative stress, osmotic stress, acidic pH, nutrient starvation, metal ions, and host antimicrobials [8]. Out of all these stresses, the bacterial peptidoglycan layer helps counter osmotic stress by acting as a barrier to the external environment and resisting internal turgor pressure, thereby preventing the cell from bursting. It also helps in maintaining the bacterial shape and virulence. The synthesis of the

46 peptidoglycan layer is a concerted effort of many proteins and takes place in the cytosolic and
47 periplasmic compartments of the bacterial cell [9]. The biosynthesis of the peptidoglycan
48 building block, N-acetylglucosamine-N-acetyl muramyl-pentapeptide, takes place in the
49 cytoplasm on the lipid carrier undecaprenyl phosphate (C_{55}-P), forming Lipid II. Lipid II is
50 then flipped by MurJ to the periplasmic phase [9], [10]. In the periplasmic phase, the
51 disaccharide pentapeptide part of Lipid-II undergoes polymerisation by SEDS (Shape,
52 Elongation, Division, and Sporulation) proteins (such as FtsW and RodA) and Penicillin-
53 binding proteins (PBPs) for peptidoglycan synthesis, releasing undecaprenyl pyrophosphate
54 [11], [12], [13], [14]. The undecaprenyl pyrophosphate (C_{55}-PP) is dephosphorylated by
55 undecaprenyl pyrophosphate phosphatase (UppP) to undecaprenyl phosphate in the
56 periplasmic phase, which is recycled for another round of peptidoglycan synthesis [15]. While
57 UppP accounts for approximately 75% of this phosphatase activity in *E. coli*, the remaining
58 activity is provided by the functionally redundant PAP2 family proteins, PgpB, YbjG, and LpxT
59 [16], [17].

60 Certain studies have highlighted the crucial role of undecaprenyl pyrophosphate phosphatases
61 in the virulence and pathogenesis of different bacterial species. In *E. coli,* the undecaprenyl
62 pyrophosphate phosphatase encoded by the gene *uppP*, also known as *bacA*, leads to bacitracin
63 resistance when it is overexpressed. Bacitracin strongly binds to undecaprenyl pyrophosphate
64 and prevents its dephosphorylation [18]. Mutant strains lacking the *bacA* homologue in
65 *Staphylococcus aureus* and *Streptococcus pneumoniae* exhibited reduced virulence and severe
66 attenuation, respectively, in the mouse model of infection [19]. HupA, an undecaprenyl
67 pyrophosphate phosphatase of the PAP2 family, belonging to *Helicobacter pylori*, is essential
68 for colonisation of the stomach [20]. Other reports have shown that deletion of *uppP* in
69 *Mycobacterium smegmatis* impairs its ability to form biofilms [21]. However, the role of

70 undecaprenyl phosphate in *Salmonella* Typhimurium (STM) pathogenesis has remained
71 unexplored.

72 Recent studies suggest that intracellular *Salmonella* actively remodels its peptidoglycan layer
73 to survive in the intracellular niche, differing significantly from those grown in LB medium
74 [22], [23]. Intracellular *Salmonella* Typhimurium actively edits its peptidoglycan to incorporate
75 elevated levels of L-alanine-D-glutamic acid (L, D-) cross-links, replacing the terminal D-
76 alanine with the amino alcohol alaninol and cleaving γ-D-glutamyl-meso-diaminopimelic acid
77 (D, D-) crosslinks, which reduce the release of immunogenic muropeptides, thereby limiting
78 recognition by innate immune receptors, such as NOD1/2, and attenuating the inflammatory
79 response [24], [25]. Additionally, in *Salmonella* Typhi, the elevated levels of L, D-crosslinks
80 play a dual role by facilitating the secretion of the typhoid toxin [22]. UppP's crucial function
81 in peptidoglycan synthesis suggests that it may play a role in cell wall adaptation during stress,
82 thereby enhancing *Salmonella*'s survival. In this study, we generated an *uppP* knockout strain
83 of *S.* Typhimurium and evaluated its impact on bacterial survival and virulence. Our findings
84 demonstrate that UppP is essential for *S.* Typhimurium proliferation in RAW 264.7
85 macrophages and systemic dissemination in C57BL/6 mice by promoting resistance to host-
86 induced nitrosative stress.

87 **Results**

88 **UppP affects bacterial cell dimensions and strength**

89 To investigate the role of undecaprenyl pyrophosphate phosphatase in *Salmonella*
90 pathogenesis, we generated an *uppP*-deleted strain of *Salmonella* Typhimurium by a one-step
91 chromosomal gene inactivation method [26]. We observed that the *uppP* deleted strain
92 demonstrated no significant difference in growth in nutrient-rich LB broth (Fig. 1A), M9

93 minimal media (Fig. 1B) and acidic F-media (pH-5.4, similar to the pH of the *Salmonella*-
94 containing vacuole [SCV]) [27], [28] (Fig. 1C).

95 A continuous supply of undecaprenyl phosphate is crucial for normal cell shape maintenance
96 in *Escherichia coli*, and its depletion induces morphological defects [29], [30], [31]. To
97 dissect the contribution of UppP in bacterial cell morphology of *Salmonella*, we performed
98 Scanning Electron Microscopy (SEM) to examine the logarithmic (1:100 dilution) and
99 stationary-phase cultures of STM WT and STM Δ*uppP*. The quantitative analysis of cell
100 length revealed that STM Δ*uppP* (1.319 ± 0.3145 μm) exhibits reduced cell length in
101 comparison to STM WT (1.509 ± 0.5406 μm) during the log phase, which was restored upon
102 complementation of *uppP* (1.768 ± 0.4086 μm) (Fig. 1D-E). Whereas there is an increase in
103 cell length of STM Δ*uppP* (1.236 ± 0.2295 μm) in comparison to STM WT (1.067 ± 0.2360
104 μm) during the stationary phase (S1A-B). Interestingly, when STM Δ*uppP* cells were
105 subcultured at a higher dilution of 1:1000, allowing them to grow for a longer period in the
106 logarithmic phase, we observed that the mutant (1.963 ± 0.5102 μm) became notably more
107 elongated compared to the wild type (1.642 ± 0.4547 μm). Additionally, cell size returned to
108 normal upon complementation (1.704 ± 0.4999 μm) (Fig. S1C-D).

109 Furthermore, we performed atomic force microscopy (AFM) to evaluate the stiffness of the
110 bacterial cell envelope. Young's modulus, quantified from AFM micrographs, was reduced in
111 the STM Δ*uppP* (39.55 ± 23.26 MPa) strain compared to the wild type (137.5 ± 115.5 MPa),
112 and this reduction was also restored upon complementation (210.3 ± 126.2 MPa) (Fig. 1F-G,
113 S1E). Additionally, we evaluated the porosity of the outer membrane through a bisbenzimide
114 uptake assay, as it is a major determinant of the stiffness of the bacterial cell envelope [32]. We
115 observed no significant difference in fluorescence uptake between the wild-type and the
116 mutant, either during the stationary or logarithmic phase (Fig. S1F). Our results indicate that
117 *uppP* contributes to the maintenance of bacterial cell size and strength.

118 To investigate whether the observed defects in bacterial cell length and stiffness of STM Δ*uppP*
119 can be attributed to biochemical changes in the cell envelope, we evaluated the composition of
120 two major components: the peptidoglycan layer and lipopolysaccharide (LPS), both of which
121 are dependent on undecaprenyl phosphate for their biosynthesis. The muropeptide composition
122 of STM WT and STM Δ*uppP* analysed using HPLC revealed no significant differences in the
123 muropeptide profile or peptidoglycan cross-links (Figure S2A-C). Similarly, silver staining of
124 LPS showed no differences in the banding pattern or intensity between the wild-type and the
125 mutant (Fig. S2D). Collectively, our results suggest that deletion of *uppP* has an impact on
126 bacterial cell morphology and stiffness, without influencing the biochemical composition of
127 either the peptidoglycan layer or lipopolysaccharide (LPS).

128 ***uppP* plays a role in the intracellular survival of *Salmonella* in RAW 264.7 macrophages**

129 As macrophages play a crucial role in the dissemination of *Salmonella* within the host, we
130 performed an intracellular survival assay using the murine macrophage-like cell line RAW
131 264.7. We assessed the percentage of phagocytosis/invasion, which represents the percentage
132 of bacteria from the total pre-inoculum that invade the cell, and fold proliferation, which
133 accounts for the extent of bacterial replication occurring inside the cell with respect to an early
134 time point, respectively. We found that STM Δ*uppP* exhibits impaired invasion and fold
135 proliferation compared to STM WT in RAW264.7 cells. The decreased percentage invasion
136 and fold proliferation of the mutant is rescued upon complementation of the *uppP* gene (Fig.
137 2A, S3A). Since the intestinal epithelial barrier is *Salmonella*'s initial point of contact, we also
138 evaluated the intracellular survival of STM Δ*uppP* in Caco-2 cells. However, we observed no
139 significant difference in the invasion or fold proliferation of STM Δ*uppP* compared to wild-
140 type in Caco-2 cells (Fig. S3B-C).

141 As SPI-1 can also contribute to macrophage invasion [33], we evaluated the transcript levels
142 of SPI-1 genes. We observed increased *sipA* (SPI-1 effector), *invF*, *hilA* (transcriptional
143 regulators), and *prgH* (structural translocon component) transcripts in the mutant during both
144 the logarithmic (6h) and stationary phase (12h) (Fig. S3D-E). Increased expression of SPI-1
145 genes is also associated with macrophage apoptosis during *Salmonella* infection [34], [35],
146 [36]. We hypothesised that the reduced invasion and fold proliferation of STM *ΔuppP* may be
147 attributed to the infected cells undergoing apoptosis. To evaluate the same, 16 hours post-
148 infection, RAW 264.7 cells were treated with tetracycline, followed by an MTT (3-(4,5-
149 dimethylthiazol-2-yl)-2,5-diphenyltetrazolium bromide) assay to determine cell viability. No
150 significant difference was observed in the cell viability between the wild-type, mutant and
151 uninfected control (Fig. S3F). This suggests that apoptosis, or other forms of cell death, may
152 not account for the decreased invasion and proliferation of STM Δ*uppP*.

153 *Salmonella* Pathogenicity Island (SPI)-2 is a key player in governing *Salmonella* survival in
154 macrophages [37]. Since STM Δ*uppP* exhibited reduced fold proliferation in RAW 264.7
155 macrophages, we evaluated the transcript levels of SPI-2 effectors *sifA* and *spiC*. Interestingly,
156 STM Δ*uppP* exhibited elevated transcripts of *sifA* and *spiC* during the stationary phase,
157 compared to the wild-type (Fig. S3G).

158 Multiple host defences within the macrophage, such as acidic pH, reactive oxygen species,
159 reactive nitrogen species, antimicrobial peptides, nutrient deprivation, etc, influence
160 *Salmonella* survival [8]. We assessed the susceptibility of STM Δ*uppP* to exogenous stresses
161 of hydrogen peroxide, nitrite and peroxynitrite by a resazurin dye-assisted cell viability assay.
162 Despite exhibiting elevated reactive oxygen species (ROS) levels, as measured by H_2DCFDA
163 staining, STM Δ*uppP* displayed only a marginal reduction in viability when subjected to
164 hydrogen peroxide stress (Fig. 2B-C). In contrast, treatment with increasing concentrations of
165 sodium nitrite and peroxynitrite resulted in significantly decreased viability of STM Δ*uppP*

166 compared to the wild-type. (Fig. 2D-G). Additionally, complementing *uppP* in the mutant strain
167 restored bacterial viability when exposed to nitrite stress (Fig. S3H). We evaluated intracellular
168 nitric oxide production in STM Δ*uppP* under sodium nitrite stress using DAF_2DA staining.
169 Flow cytometry-mediated visualisation showed that STM Δ*uppP* demonstrates an increased
170 percentage of DAF_2DA-positive cells upon nitrite stress (Fig. 2H-I). Moreover, on exposure to
171 nitrite stress, STM Δ*uppP* exhibited an elevated median fluorescence intensity (MFI) compared
172 to the wild type, indicating elevated nitric oxide levels (Fig. 2J). Our findings suggest that UppP
173 contributes to *Salmonella* survival in RAW264.7 cells by aiding the bacterial defence against
174 nitrosative stress.

175 **UppP deletion leads to increased nitric oxide (NO) production and nitrotyrosine**
176 **localisation with intracellular bacteria within macrophages**

177 To evaluate if the reduced fold proliferation of STM Δ*uppP* is attributed to nitrosative stress,
178 we measured nitric oxide production by infected macrophages. We performed the Griess assay
179 to evaluate the levels of extracellular NO in the culture supernatants of RAW 264.7 cells
180 infected with STM WT, STM Δ*uppP* and STM Δ*uppP:uppP* for 16 hours. There was an 8 to
181 10-fold increase in the extracellular nitrite concentration in the culture supernatants of RAW
182 264.7 cells infected with STM Δ*uppP* (38.19 ± 5.025 μM) in comparison to the wild-type
183 control (3.949 ± 1.418 μM). Moreover, upon complementation of *uppP*, the extracellular nitrite
184 levels were restored (3.172 ± 1.006 μM), similar to that of the wild-type (Fig. 3A). We infected
185 RAW 264.7 cells with STM WT and STM Δ*uppP,* transformed with the pFPV-mCherry
186 plasmid, responsible for the constitutive expression of mCherry [38]. This was followed by
187 DAF_2DA staining 16h post-infection. The STM Δ*uppP*-mCherry infected cells showed
188 increased MFI compared to STM WT-mCherry infected cells, indicating elevated nitric oxide
189 levels (Fig. 3B-C, S4A-C). To verify that the elevated NO production was specifically STM
190 Δ*uppP:uppP* for 16h, followed by DAF_2DA staining. We observed increased intracellular NO

levels in STM Δ*uppP*-infected cells, which were restored to wild-type levels upon complementation (Fig. S4D-E). NO exerts its bactericidal activity by oxidising to form NO adducts, such as nitrites and peroxynitrites, with peroxynitrite nitrosylating tyrosine and impairing protein function [39]. To assess this, we used confocal laser scanning microscopy to estimate nitrotyrosine levels in RAW 264.7 cells 16h post-infection with eGFP-tagged STM WT and STM Δ*uppP*. Our results show that in comparison to STM WT, there is an increase in the colocalisation of nitrotyrosine residues with STM Δ*uppP*. Moreover, cells infected with STM Δ*uppP* demonstrated increased levels of nitrotyrosine residues, consistent with our flow cytometry findings (Fig. 3D-F). To further solidify our findings, we performed an ELISA to quantify nitrotyrosine residues in the lysates of RAW 264.7 cells infected with STM WT, STM Δ*uppP* and STM Δ*uppP:uppP* for 16h. The cell lysates of STM Δ*uppP*-infected cells exhibited increased levels of nitrotyrosine residues, which reverted to wild-type levels upon complementation of *uppP* (Fig. S4F). Taken together, the elevated nitric oxide and nitrotyrosine levels in RAW 264.7 cells infected with STM Δ*uppP* suggest that *uppP* may have a protective role against nitrosative stress.

Elevated NO production is also a prominent indicator of M1 polarised proinflammatory macrophages [40]. To determine whether the increased NO production resulted from a heightened immune response against the mutant, hence aiding in bacterial clearance, we quantified the levels of *Nos2* transcript and two other proinflammatory markers, CD86 and TNF-α, using flow cytometry and ELISA, respectively. The *Nos2* gene encodes for the enzyme inducible nitric oxide synthase (iNOS), which generates NO. We observed that the *Nos2* mRNA transcript was elevated in RAW 264.7 cells upon infection with STM Δ*uppP* in comparison to STM WT (Fig. 3G). Flow cytometry analysis showed that there was an increase in the MFI of STM Δ*uppP*-infected RAW 264.7 cells in comparison to the STM WT and STM Δ*uppP:uppP*-infected cells, indicating a higher cell surface expression of CD86 upon infection with STM

216 Δ*uppP* (Fig. S5A-B). Additionally, we observed that the spent media of RAW 264.7 cells
217 infected with STM Δ*uppP* showed a minimal increase in TNF-α levels compared to STM WT-
218 infected cells (Fig. S5C). Altogether, these data indicate that STM Δ*uppP* may exhibit increased
219 immunogenicity, inducing a stronger proinflammatory immune response within host
220 macrophages in comparison to STM WT. This NO-driven immune response, along with the
221 mutant's innate sensitivity to nitrosative stress, may facilitate its clearance in macrophages.

222 **UppP mutant shows increased survival on alleviating nitrosative stress**

223 To corroborate our findings of *uppP*'s role in withstanding nitrosative stress, we inhibited
224 inducible nitric oxide synthase (iNOS) by an irreversible inhibitor, 1400W [27], [41], and
225 observed a rescue in the fold proliferation of STMΔ*uppP* in RAW 264.7 cells (Fig. 4A).

226 To investigate the role of *uppP* in *Salmonella* pathogenesis *in vivo*, C57BL/6 mice were orally
227 challenged with a dose of 10^7 CFU of STM WT, and STM Δ*uppP* and bacterial burden was
228 assessed 5 days post-infection (Fig. S6A). STM Δ*uppP* displayed reduced dissemination by
229 blood and decreased bacterial loads in the intestine, MLN (mesenteric lymph node), liver and
230 spleen (Fig. S6B-F). Additionally, STM Δ*uppP*-infected mice demonstrated a modest increase
231 in survival compared to STM WT (Fig. S6G). Furthermore, to evaluate whether the mutant's
232 attenuation in the mouse model was due to its increased susceptibility to nitrosative stress,
233 *iNOS*$^{-/-}$ C57BL/6 mice were orally challenged with 10^5 CFU of STM WT and STM Δ*uppP*
234 (Fig. S6H). Notably, STM Δ*uppP* still exhibited attenuation in dissemination and reduced organ
235 burden compared to the wild type (Fig. S6I-M). These findings suggest that UppP may have
236 additional roles in bacterial invasion of the intestine, beyond its role in conferring resistance to
237 nitrosative stress. To specifically evaluate UppP role in countering nitrosative stress during
238 systemic infection, *iNOS*$^{+/+}$ and *iNOS*$^{-/-}$ C57BL/6 mice were intraperitoneally injected with 10^4
239 CFU of STM WT and STM Δ*uppP* (Fig. 4B). We observed a significantly increased burden of

240 STM Δ*uppP* in the blood, liver and spleen of *iNOS*$^{-/-}$ mice compared to *iNOS*$^{+/+}$ mice,
241 substantiating the role of UppP in shielding *Salmonella* from nitrosative stress (Fig. 4C-E).

242 Induction of iNOS and NO production is triggered by downstream signalling from multiple
243 pattern recognition receptors (PRRs). These include but are not limited to TLR4, TLR2, NOD1,
244 and NOD2, out of which the latter of the three receptors detects various components associated
245 with the bacterial peptidoglycan layer and TLR4 recognises lipopolysaccharide (LPS) [42],
246 [43], [44], [45]. Also, both NOD1 and NOD2 have been reported to localise on *Salmonella*-
247 containing vacuole [46], [47]. As UppP is involved in the biosynthesis of both peptidoglycan
248 and LPS, we aimed to determine whether signalling through their cognate PRRs contributes to
249 the enhanced susceptibility of STM Δ*uppP* in macrophages. We inhibited TLR2, TLR4 and
250 RIPK2 (the immediate downstream kinase of NOD receptors) using small molecule inhibitors
251 C29, Restoravid and WEHI-345, respectively [48], [49], [50]. We observed a rescue in the fold
252 proliferation of STM Δ*uppP* in RAW 264.7 cells upon treatment with RIPK2 inhibitor WEHI-
253 345, but not with either C29 or Restoravid, suggesting that NOD signalling may play a role in
254 the increased susceptibility of STM Δ*uppP* in macrophages (Fig. 4F, S7A). Furthermore, to
255 identify the NOD receptor which may be involved, we estimated the transcript levels of *Nod1*
256 and *Nod2* in RAW264.7 cells infected with STM WT and STM Δ*uppP*. Although we did not
257 observe any significant difference in the transcript levels of *Nod1*, we detected elevated *Nod2*
258 transcript levels in RAW 264.7 cells, 2 hours post-infection with STM Δ*uppP* (Fig. S7B-C).

259 We performed immunofluorescence microscopy in STM WT and STM Δ*uppP*-infected
260 RAW264.7 cells to extend our findings to the translational level. We found that STM Δ*uppP*-
261 infected RAW264.7 cells at 6 and 16 hours post-infection exhibited a higher corrected total cell
262 fluorescence (CTCF) of NOD1 and NOD2, respectively, compared to the wild-type and
263 uninfected control (Fig. 4G-H, S7D-E). To further validate our findings, we treated RAW 264.7
264 cells with Nodinitib-1 and GSK717, which inhibit NOD1 and NOD2, respectively [51]. We

265 observed a rescue in the fold proliferation of STM Δ*uppP* in RAW264.7 cells, treated with
266 either Nodinitib-1 or GSK717, suggesting that both NOD1 and NOD2-mediated signalling may
267 contribute to the attenuated proliferation of STM Δ*uppP* within macrophages (Fig. 4I).

268 **Discussion**

269 Cell wall integrity is vital for bacterial structure, protection, and survival. Reports in
270 *Escherichia coli*, *Salmonella* Typhimurium and *Bacillus subtilis* have shown that cell size and
271 shape are affected by changes in growth rate and nutritional availability [52], [53], [54], [55].
272 Although the STM Δ*uppP* mutant exhibited similar growth rate kinetics to the wild type in
273 LB medium, similar to the observations of *uppP* mutant in *E. coli* [15]. However, we found
274 structural defects in STM Δ*uppP* through SEM and AFM-assisted visualisation. Quantitative
275 analysis of SEM images confirmed a biphasic effect: STM Δ*uppP* cells were shorter in
276 logarithmic phase (1:100 dilution) but longer in stationary phase than wild-type cells.
277 Interestingly, STM Δ*uppP* cells were notably more elongated than wild-type cells when
278 allowed to grow in a longer logarithmic phase (1:1000 dilution). This may stem from altered
279 surface area to volume (SA/V) ratios; increased SA/V in the low dilution (1:100) log phase
280 could permit division at smaller sizes, while the reduced surface area synthesis rate in the
281 stationary phase and the high dilution (1:1000) logarithmic phase might facilitate cell
282 lengthening, resulting in a decrease in the SA/V ratio [56], [57]. Additionally, the AFM
283 results revealed a reduced Young's modulus of STM Δ*uppP* cells. Undecaprenyl phosphate,
284 produced by the undecaprenyl pyrophosphate phosphatase activity of *uppP*, is a shared lipid
285 carrier in the biosynthesis pathways of peptidoglycan, O antigen and enterobacterial common
286 antigen (ECA), all of which contribute to the stiffness of the cell envelope to varying degrees
287 [30], [31]. Recent work has demonstrated that the outer membrane comprising O antigen and
288 ECA is a major determinant of mechanical stiffness in Gram-negative bacteria [32]. In
289 conjunction with our SEM and AFM findings, this led us to hypothesise that STM Δ*uppP*

290 may have an altered cell envelope. Interestingly, the biochemical analysis of the composition
291 of both the peptidoglycan and LPS revealed no significant differences between the mutant
292 and the wild-type strains. This suggests that the reduced Young's modulus of the mutant and
293 its biphasic morphological defects may be attributed to the availability dynamics of free
294 undecaprenyl phosphate, which may in turn affect the biosynthesis rate of these
295 macromolecules, rather than their composition or structure. Moreover, our bisbenzimide
296 uptake assay demonstrated that there was no increased outer membrane porosity in the
297 mutant, suggesting that the loss of *uppP* impairs the mechanical properties of the cell
298 envelope without affecting the outer membrane's barrier function.

299 The changes observed in the bacterial cell dimensions of STM Δ*uppP* may also contribute to
300 its attenuated virulence. Maintaining the correct cellular shape is imperative for the
301 pathogenicity of various Gram-negative bacteria. For example, peptidoglycan hydrolase
302 deletion mutants of *Helicobacter pylori* and *Campylobacter jejuni* deviate from their standard
303 helical shape to a rod or curved rod morphology, which leads to impaired colonisation in the
304 mouse and chick model, respectively [58], [59], [60]. Furthermore, Uropathogenic *E. coli*
305 (UPEC) subverts neutrophil-mediated phagocytosis by undergoing filamentation [61]. Thus,
306 the morphological alterations in STM Δ*uppP* are likely to influence its survival in *in vitro* and
307 *in vivo* settings.

308 To further explore the functional consequence of UppP during *Salmonella* pathogenesis, we
309 infected RAW 264.7 murine macrophages and Caco-2 colon carcinoma cells with the STM
310 Δ*uppP*. Though STM Δ*uppP* demonstrated no growth defects in Caco-2, its proliferation was
311 attenuated in RAW 264.7 cells. Resazurin-assisted live/ dead assay revealed that STM Δ*uppP*
312 had increased susceptibility to nitrosative stress. Moreover, inhibition of inducible nitric
313 oxide synthetase restored the proliferation of STM Δ*uppP* in macrophages. Even though
314 *Salmonella* avoids trafficking of iNOS-containing vesicles to the *Salmonella*-containing

315 vacuole (SCV) in an SPI-2-dependent manner, the freely diffusible nature of nitric oxide
316 (NO) can facilitate bacterium killing [62], [63]. The altered cell structure of the null mutant
317 may further facilitate the entry of NO within the bacterium. Also, STM Δ*uppP*-infected
318 macrophages exhibited elevated levels of NO and CD86, along with increased secretion of
319 TNF-α, suggesting that the mutant elicits a robust proinflammatory immune response within
320 macrophages. This enhanced immune response, driven by increased NO production and the
321 mutant's inherent nitrite sensitivity, may promote its attenuated survival within macrophages.

322 The nucleotide oligomerisation domain (NOD) - like receptors 1 and 2 (NOD1/2) are
323 cytoplasmic pattern recognition receptors (PRRs) recognising γ-d-glutamyl-meso-
324 diaminopimelic acid (iE-DAP) and muramyl dipeptide (MDP), which are constituents of the
325 peptidoglycan layer [64]. NOD1 and NOD2, and RIPK2 (downstream effector protein
326 kinase) are reported to colocalise with the SCV, along with endosomal transporters SLC15A3
327 and SLC15A4, which translocate MDP to NOD receptors [46], [47]. In the *Salmonella* colitis
328 model, mice deficient for NOD1 and NOD2 have higher bacterial loads in the mucosal tissue
329 [65]. *Mycobacterium tuberculosis* growth in human macrophages is controlled by NOD2-
330 dependent NO production [66]. Similarly, NOD2 induces NO, which mediates bacterial
331 clearance in the mouse model of *Chlamydophila pneumoniae*-induced pneumonia [67].
332 NOD1-induced NO production provides resistance against *Trypanosoma cruzi* in the murine
333 model [68]. TLR2 and TLR4, which recognise peptidoglycan and LPS, respectively, also
334 signal the production of NO during bacterial infections [42], [45]. Upon inhibiting RIPK2,
335 NOD1 or NOD2, but not TLR2 and TLR4, we observed a rescue in the proliferation of STM
336 Δ*uppP* in macrophages. Undecaprenyl phosphate is a common substrate for synthesising
337 peptidoglycan, O antigen, and ECA, all of which function as essential virulence determinants
338 [17]. Initially, we hypothesised that an insufficient influx of undecaprenyl phosphate may
339 lead to the accumulation of precursors and intermediates, which may act as ligands to directly

340 or indirectly activate PRRs. In our study, upon deletion of *uppP,* we did not observe any
341 difference in the composition of either LPS or peptidoglycan. We propose an alternative
342 hypothesis that the deletion of *uppP* may slow the synthesis rate of both peptidoglycan and
343 lipopolysaccharide; however, the synthesis of the latter will be more significantly impacted
344 than that of the former, as peptidoglycan is more essential to the cell envelope. The slowed
345 synthesis of peptidoglycan and LPS may explain the mutant's reduced stiffness and altered
346 morphology, leading to its lysis more quickly within macrophages. Furthermore, upon
347 bacterial lysis of the *uppP* mutant, the peptidoglycan fragments may be relatively more
348 abundant, leading to the preferential activation of NOD receptors and driving macrophage
349 activation and elevated NO levels.

350 In C57BL/6 mice with functional iNOS (*iNOS*$^{+/+}$), intraperitoneal infection with STM Δ*uppP*
351 showed reduced dissemination by blood and decreased colonisation in the spleen and liver.
352 This phenotype was reversed in iNOS-deficient mice, confirming the role of UppP in
353 promoting *Salmonella* dissemination and colonisation by counteracting nitrosative stress.

354 To the best of our knowledge, our study is one of the first to report a unique function of
355 undecaprenyl pyrophosphate phosphatase in mitigating nitrosative stress in *Salmonella* (Fig.
356 5), in addition to its canonical roles in cell envelope biogenesis and maintenance of
357 morphology. Our findings potentially highlight undecaprenyl phosphate metabolism as a
358 promising target for developing new antimicrobial strategies to enhance the efficacy of
359 macrophage-mediated clearance of *Salmonella* infection.

360 **Material and methods**

361 **Bacterial strains and growth condition:** *Salmonella enterica* serovar Typhimurium 14028S
362 (STM WT) was used in all experiments. Bacterial strains were cultured in Luria Bertani (LB)
363 broth (HiMedia) with constant shaking (160 rpm) at 37°C (wild type, knockout strains) or 30°C

364 (strains having temperature-sensitive pKD46 plasmid). Ampicillin (50µg/ml), Kanamycin
365 (50µg/ml), Chloramphenicol (25µg/ml) and IPTG (500µM) were used wherever required. A
366 complete list of bacterial strains and plasmids used in this study is provided in Table 1.

367 Table 1. Strains and plasmids used in this study

Strains/ Plasmids	Characteristics	Source/ Information
Salmonella enterica subspecies *enterica* serovar Typhimurium strain 14028S	Wild type (WT)	Gift from Prof. M. Hensel (Division of Microbiology, University of Osnabrück, Germany)
STMΔ*uppP*	Chl^R	This study
STM Δ*uppP:uppP* (STMΔ*uppP*:pQE60:*uppP*)	Chl^R, Amp^R	This study
STM:pFPV-mCherry	Constitutive expression of mCherry in STM WT, Amp^R	Laboratory stock
STMΔ*uppP*:pFPV-mCherry	Constitutive expression of mCherry in STM Δ*uppP*, Amp^R, Chl^R	This study
STM:pFPV25.1	Constitutive expression of GFP in STM WT, Amp^R	Laboratory stock
STMΔ*uppP*:pFPV25.1	Constitutive expression of GFP in STM Δ*uppP*, Amp^R, Chl^R	This study
pKD3	Plasmid with FRT flanked by Chloramphenicol-resistance gene, Chl^R	Laboratory stock
pKD46	Plasmid expressing λ red recombinase system, Amp^R	Laboratory stock
pQE60	Low copy number plasmid, Amp^R	Laboratory stock
pFPV-mCherry	Constitutive expression of mCherry, Amp^R	Laboratory stock
pFPV25.1	Constitutive expression of GFP, Amp^R	Laboratory stock

368 **Construction of *uppP* knockout strain of *Salmonella*:** The knockout strain of *Salmonella*
369 enterica serovar Typhimurium (strain 14028S) was generated using the one-step chromosomal
370 gene inactivation method developed by Datsenko and Wanner [26]. In a concise overview, STM
371 WT was transformed with pKD46 plasmid, housing a 'lambda red recombinase system'
372 controlled by an arabinose-inducible promoter. The transformed cells were cultivated in LB
373 broth with ampicillin (50 µg/mL) and 50 mM arabinose at 30°C until an optical density of 0.35
374 to 0.4 at 600nm. Electrocompetent STM pKD46 cells were prepared by washing the bacterial
375 cell pellet thrice with double autoclaved chilled Milli Q water and 10% (v/v) glycerol. Finally,
376 the electrocompetent STM pKD46 cells were resuspended in 50 µL of 10% glycerol. For the
377 knockout procedure, the chloramphenicol-resistant gene cassette (Chl^R, 1.1 kb, used for
378 knocking out *uppP*) was amplified from the pKD3 plasmid, utilising knockout primers. The
379 amplified Chl^R gene cassettes underwent chloroform-isopropanol extraction and were
380 electroporated into STM WT pKD46. The transformed cells were then plated on LB agar with
381 chloramphenicol (25 µg/mL) to select the STM*ΔuppP* strain. Subsequently, the plates were
382 incubated overnight at 37°C. The confirmation of knockout colonies was achieved through
383 expression primers. The primers used for generating the knockout strain are listed in Table 2.

384 **Construction of *uppP* complemented strain of *Salmonella*:** The *uppP* gene was amplified
385 using cloning primers through colony PCR. The resulting PCR product, purified via chloroform
386 extraction, was then subjected to EcoRI (NEB) and HindIII (NEB) restriction digestion in
387 CutSmart buffer (NEB) at 37°C overnight, alongside the empty pQE60 vector backbone. The
388 double-digested insert and vector were ligated using T4 DNA ligase in 10X ligation buffer
389 (NEB) overnight at 16°C. The ligated product was subsequently transformed into the knockout
390 strains to generate the complemented strain. Verification of complementation was
391 accomplished through the restriction digestion of the recombinant plasmid and Sanger
392 sequencing. The primers used for generating the complement strain are listed in Table 2.

393 Table 2. List of primer sequences (5’ to 3’)

Primer Name	Sequence (5’ to 3’)
uppP KO FP	CCAAACGGTTATATATGGGGTCTTAACGCGAGATCCATTTCATATGAATATCCTCCTTAG
uppP KO RP	GCCATCCGGCACGGTCAATCATCAGAAGAAGACAACGTAAGTGTAGGCTGGAGCTGCTTC
uppP confirmatory FP	ATTGAGCGTGGCAATAATCTG
uppP confirmatory RP	CTGCGCTTATCAGACCGACAA
uppP cloning FP	GCGAATTCAGGAGAATGAGCGATATGCACTCGCTGCTG
uppP cloning RP	GCAAGCTTTCAGAAGAAGACAACGTAAACGG
16S rRNA RT FP	CGCTTCTCTTTGTATGCGCC
16S rRNA RT RP	TCGTCAGCTCGTGTTGTGAA
spiC RT FP	AGGGCCGAAGGTAATAGCCGA
spiC RT RP	CCCATCCGCTGTGAGCTGTA
sifA RT FP	TCGCATCCACAAATGACGGC
sifA RT RP	TTCGCTGCCAGGTAGGTTGC
hilA RT FP	GCCGGTGACCATTACGAAGA
hilA RT RP	AAGAGAGAAGCGGGTTGGTG
sipA RT FP	TTCGGATGAAGCGTTGGTCA
sipA RT RP	GTCATTCGCGTGTGGATTCG
invF RT FP	CGTCGTTTGTGCAGCAGAGC
invF RT RP	TAATTTCCGCGGCGAAACGC
prgH RT FP	CGTTTTCAGGTGTTGCCAGG
prgH RT RP	TACGCGGCTCATCGAAATGA
β-actin RT FP	GGTGGGAATGGGTCAGAAGG

β-actin RT RP	AGGTCTCAAACATGATCTGGGT
Nod1 RT FP	CCTCAAGCACCTTAAACTAGGGA
Nod1 RT RP	TCCTTCAATGCCTCTGCGAA
Nod2 RT FP	ACTGTCCAACAATGGCATCAC
Nod2 RT RP	TGTGTTCCCTCGAAGCCAAA
Nos2 RT FP	AGCCACAGTCCTCTTTGCT
Nos2 RT RP	ACAACCTGTGTGACAACCGT

Growth Curve Analysis: For *in vitro* growth curve experiments, a single colony of each strain was inoculated in Luria Bertani (LB) broth (HiMedia) with constant shaking (160 rpm) at 37°C, with the corresponding antibiotic. Overnight-grown stationary phase bacteria were sub-cultured at a ratio of 1: 100 in freshly prepared LB broth, M9 minimal media and F-media (50mM KCl, 75mM $(NH_4)SO_4$, 5mM K_2SO_4 10mM K_2HPO_4, 1Mm Bis-Tris, 8μM $MgCl_2$, 38mM glycerol and 0.1% cas amino acids, pH- 5.4) kept at 37ºC, with constant shaking (160 rpm). At different time intervals, aliquots were taken to measure [OD]595nm by TECAN 96 well microplate reader or for CFU analysis.

Scanning electron microscopy (SEM): Overnight cultures were subcultured in LB broth at a 1:100 or 1:1000 ratio for 5-6 hours to obtain logarithmic-phase cultures. Logarithmic phase bacterial cultures were drop-casted and immobilised over coverslips by air-drying, followed by overnight fixation with 3.5% glutaraldehyde at 4°C. The following day, the samples were washed with MilliQ water and treated with an increasing ethanol gradient (10%, 30%, 50%, 70%, 90%, and 100%) to facilitate dehydration. The samples were desiccated for 30 minutes, mounted on copper stubs using carbon tape and coated with gold particles under high vacuum.

410 Images were acquired with an ESEM Quanta microscope at a magnification of 5000X. ImageJ
411 was used to analyse bacterial size.

412 **AFM (Atomic force microscopy):** AFM-mediated assessment of bacterial morphology was
413 performed by adopting the protocol from [69]. Overnight cultures were subcultured in LB broth
414 at a 1:100 ratio for 5-6 hours to obtain logarithmic-phase cultures. Logarithmic phase bacterial
415 cultures were drop-casted and immobilised over coverslips by air-drying, followed by fixation
416 with 3.5% paraformaldehyde. The samples were washed thrice with MilliQ water, followed by
417 desiccation for 30 minutes. Images were acquired from an NX10 AFM. XEI software was
418 utilised to calculate Young's modulus.

419 **Bisbenzimide assay to determine the outer membrane porosity of bacteria:** The outer
420 membrane porosity of the bacterial strains (STM WT, STM Δ*uppP*, and STM Δ*uppP:uppP*) in
421 both the stationary phase and logarithmic phase was measured using bisbenzimide (Sigma-
422 Aldrich), as modified from a previously specified protocol [27], [70]. At the end of the
423 incubation period, the OD_{600nm} of the cultures was adjusted to 0.1 with sterile 1x PBS.
424 Subsequently, 180 µL of 0.1 OD culture was added to a 96-well microplate containing 20 µl of
425 bisbenzimide (10 µg/mL) solution and further incubated for 10 minutes at 37°C in a shaker
426 incubator. Due to enhanced outer membrane porosity, when bisbenzimide is taken up by
427 bacterial cells, it binds to the bacterial DNA and begins to fluoresce. The fluorescence intensity
428 of DNA-bound bisbenzimide was measured in a TECAN 96-well microplate reader using 346
429 nm excitation and 460 nm emission filter.

430 **Peptidoglycan isolation and analysis:** The isolation and analysis of peptidoglycan were
431 performed as described in [71], [72], [73]. Overnight bacterial cultures were subcultured at a
432 1:100 dilution in 500 mL of LB broth. Bacterial strains were grown till the logarithmic phase
433 ($OD_{600nm} \approx 1$) and subsequently harvested by centrifugation at 8000 RPM for 20 minutes at

434 4°C. The cell pellet was resuspended in chilled MQ water, and the suspension was added
435 dropwise to an equal volume of a constantly boiling solution of 8% SDS. The suspension was
436 boiled for an additional 40 minutes, with continuous stirring and allowed to cool overnight at
437 RT. The sample was mixed with MQ water and pelleted by ultracentrifugation at 3,00,000g,
438 for 90 minutes, at RT. After multiple washes to completely remove SDS, the pellet was
439 resuspended in 10 mM Tris Cl pH 7, 10mM NaCl buffer and treated with 0.1 mg/mL of α-
440 amylase for 2 hours at 37°C, followed by treatment with 0.2 mg/mL of pronase for 2 hours at
441 60°C. The enzymes were inactivated by boiling with an equal volume of 8% SDS for 20
442 minutes, followed by removal of SDS, with several washes of MQ water by centrifugation at
443 25,000g at RT. The peptidoglycan pellets were finally resuspended in 25 mM Tris-HCl, pH 8,
444 and stored at -30°C.

445 For analysing the peptidoglycan composition, muropeptide fragments were obtained by
446 digesting the peptidoglycan with 10 U of mutanolysin in a 25 mM Tris-HCl buffer, pH 8, at
447 37°C for 16 hours. The samples were centrifuged at 25,000g for 10 minutes at RT, and the
448 supernatant comprising the soluble muropeptides was reduced with 1 mg of sodium
449 borohydride in 50 mM sodium-borate buffer, pH 9, for 30 min. 88% ortho-phosphoric acid was
450 added to decrease the pH to 2, thereby eliminating the excess borohydride. The sample was
451 centrifuged to remove any additional particulate matter, and the supernatant was injected into
452 a preheated (55°C) Zorbax 300SB RP-C18 column, connected to an Agilent Technologies
453 RRLC 1200 HPLC system. Muropeptides were eluted using a 0 to 20% gradient of acetonitrile
454 containing 0.1% trifluoroacetic acid with a flow rate of 0.5 mL/min for 80 minutes.
455 Muropeptides were detected by measuring absorbance at 205 nm.

456 **LPS isolation and quantification:** The isolation and quantification of LPS were performed
457 according to the protocol described by Mahalakshmi et al [74]. Cell lysates were prepared by
458 sonication of logarithmic-phase strains (STM WT, STM Δ*uppP*, and STM Δ*uppP:uppP*)

459 resuspended in 10mM HEPES buffer (pH 7.4). The protein concentration of the cell lysates
460 was estimated using the Bradford Reagent (Bio-Rad) with standard solutions comprising
461 bovine serum albumin (BSA) concentrations ranging from 50 μg/μL to 0.31 μg/μL. Equal
462 volumes of cell lysates, normalised to protein content, were mixed with an equal volume of
463 tricine sample buffer (comprising 100 mM Tris-HCl, pH 6.8, 24% w/v glycerol, 8% w/v SDS,
464 5% v/v 2-β-mercaptoethanol, and 0.02% w/v bromophenol blue) and boiled for 10 minutes. 10
465 μL of proteinase K solution (2.5 mg/mL in sample buffer) was added to 50 μL of the boiled
466 sample, followed by incubation at 60°C for 1 hour. Subsequently, the sample was centrifugation
467 at 16,000 g for 30 minutes. The supernatants were loaded onto 16.5% tricine-SDS
468 polyacrylamide gels, and LPS was visualised through silver staining.

469 **Cell culture protocol:** DMEM- Dulbecco's Modified Eagle Medium (Lonza) supplemented
470 with 10% FBS (Gibco) was used to culture RAW 264.7 murine macrophages and the human
471 colorectal adenocarcinoma cell line, Caco-2. The cells were maintained at 37°C in a humified
472 incubator with 5% CO_2. Additionally, Caco-2 cells were supplemented with 1% sodium
473 pyruvate (Sigma) and 1% non-essential amino acids (Sigma). Cells were seeded at a density of
474 1.5 x 10^5 cells per well in a 24-well plate for intracellular survival assay preceding infection.

475 **Gentamicin protection assay:** Macrophages or epithelial cells were infected with stationary-
476 phase or logarithmic phase bacterial culture with an MOI of 10. For synchronisation of the
477 infection and enhancing bacterial adhesion, tissue culture plates were centrifugated at 600 rpm
478 for 5 minutes, followed by incubation for 25 minutes at 37°C in a humified incubator with 5%
479 CO_2. Post-incubation cells were washed with 1X PBS, and fresh media (DMEM + 10% FBS)
480 containing 100μg/ml gentamicin was added, followed by 1h of incubation at 37°C and 5% CO_2.
481 Subsequently, the gentamicin concentration was reduced to 25μg/ml and maintained until the
482 cells were harvested.

483 **Percentage phagocytosis and Intracellular proliferation:** Following infection of cells with
484 STM at an MOI of 10, cells were treated with DMEM (Sigma) supplemented with 10% FBS
485 (Gibco) containing 100µg/ml gentamicin for 1h. Subsequently, the gentamicin concentration
486 was reduced to 25µg/ml and maintained until the specified time point.

487 Additionally, in some experiments, 1400W dihydrochloride (Sigma), an inhibitor for inducible
488 nitric oxide synthetase (iNOS), or WEHI-345 (MedChemExpress, HY-18937), a RIPK2
489 inhibitor which delays NOD signalling [50], Nodinitib-1 (MedChemExpress, HY-18639), an
490 inhibitor of NOD1, and GSK717 (MedChemExpress, HY-136555), an inhibitor of NOD2, were
491 administered to cells at concentrations of 10µM, 1µM, 5µM, and 5µM respectively, alongside
492 25µg/ml gentamicin treatment. TLR2 and TLR4 were inhibited using C29 (MedChemExpress,
493 HY-100461) and Resatorvid (MedChemExpress, HY-11109), respectively, at concentrations of
494 25 µM and 100 nm. The cells were treated with either C29 or Resatorvid for 4 hours prior to
495 infection, followed by the addition of the inhibitor alongside the 25µg/ml gentamicin during
496 the entire infection period. 2h and 16h post-infection; cells were lysed in 0.1% triton-X-100.
497 Lysed cells and the pre-inoculum were serially diluted and plated onto LB agar or *Salmonella-*
498 *Shigella* agar to obtain colony-forming units (CFU). Calculations for percentage phagocytosis/
499 invasion and fold proliferation are as follows:

500 $$Percentage\ Phagocytosis\ or\ Invasion\ = \frac{No.\ of\ CFU\ at\ 2h}{No.\ of\ CFU\ in\ Pre\ inoculum} \times 100$$

501 $$Fold\ Proliferation\ = \frac{No.\ of\ CFU\ at\ 16h}{No.\ of\ CFU\ at\ 2h}$$

502 **RNA isolation and quantitative RT PCR:** Bacterial strains were inoculated in LB broth,
503 followed by subculture in LB broth at a ratio of 1:100. Bacterial cells were pelleted and lysed
504 in TRIzol (RNAiso plus Takara). Total RNA was isolated from the TRIzol lysed sample as per
505 the manufacturer's protocol. Quantification of RNA was performed in NanoDrop (Thermo-
506 Fischer Scientific). The quality of isolated RNA was detected by performing gel electrophoresis

507 with 2% agarose gel. 1µg of RNA was subjected to Turbo DNase (Thermo-Fischer Scientific)
508 treatment at 37°C for 30 minutes, followed by the addition of EDTA and heat inactivation at
509 65°C for 10 mins. The mRNA was reverse transcribed to cDNA using oligo dT primer, random
510 hexamers, buffer, dNTPs, and reverse transcriptase (Takara) as per the manufacturer's protocol.
511 The expression profile of target genes was evaluated using specific primers by using TB green
512 RT-qPCR master mix (Takara) in the Applied Biosystem QuantStudio-5 system. 16S rRNA and
513 β-actin were used as internal controls for bacterial and host genes, respectively. All the
514 reactions were set up in 384-well plates with three replicates for each sample. The primers used
515 for RT-qPCR are listed in Table 2 [75], [76], [77].

516 **MTT Assay:** Post 16h of infection, cells were treated with complete media containing 10µg/ml
517 tetracycline for one hour to kill the intracellular bacteria, to negate the influence of MTT (3-
518 (4,5-dimethylthiazol-2-yl)-2,5-diphenyltetrazolium bromide) metabolisation by the bacteria
519 [78]. On completion of the tetracycline treatment, fresh incomplete media (i.e. DMEM only)
520 containing 0.5mg/ml MTT (Sigma) was added to cells, followed by 3h of incubation at 37°C
521 and 5% CO2 in the dark. After incubation, media is removed, and DMSO is added, followed
522 by proper aspiration to dissolve the formazan dye. The optical density was measured at 590nm.

523 **Intracellular Reactive oxygen species (ROS) determination using H_2DCFDA staining:**
524 Overnight cultures were inoculated into fresh LB media. Upon reaching an optical density of
525 0.1 (logarithmic phase), H_2DCFDA was added at a final concentration of 10µM to 10^8 CFU/ml
526 of each strain in 1xPBS (pH 7.2) and incubated at 37°C for 30 minutes. Subsequently, 10^7
527 H_2DCFDA-stained bacterial cells were suspended in 1xPBS (pH 7.2) containing varying
528 concentrations of hydrogen peroxide (1-5mM) and incubated at 37°C with orbital shaking for
529 2 hours. The samples were then transferred to a 96-well ELISA plate, and fluorescence was
530 quantified using a Tecan-ELISA plate reader. (Ex-490nm/ Em-520nm).

531 **Bacterial nitric oxide (NO) determination using DAF-2DA staining:** The production of
532 nitric oxide (NO) indicates nitrosative stress. We evaluated the NO generation of the strains to
533 *in vitro* nitrite stress by staining with DAF2-DA (4, 5- diamino fluorescein diacetate). DAF2-
534 DA is a cell membrane-permeable dye that forms a membrane-impermeable adduct emitting
535 fluorescence in NO presence. To mimic nitrite stress *in vitro*, 10^8 CFU/ml of bacteria were
536 treated with a range (500µM-5mM) of acidified nitrite (NaNO2 in PBS of pH 5.4) and
537 incubated for 12 hours at 37°C. Post incubation, the cells are treated with 5µM DAF-DA and
538 incubated for 30 minutes at 37°C. BD FACSverse flow cytometer was used to acquire the
539 samples (Ex-491nm/ Em-513nm).

540 **Resazurin assay:** Resazurin dye was used to evaluate the viability of bacteria when subjected
541 to *in vitro* peroxide stress, acidified nitrite and peroxynitrite stress. 10^8 CFU/ml of bacteria
542 were treated with varying concentrations of H_2O_2 (1-5mM) and acidified nitrite (500µM-
543 5mM), simulating oxidative and nitrosative stress, respectively. For peroxynitrite stress, a
544 combination of H_2O_2 and acidified nitrite was used in a combined concentration range of
545 62.5µM -1mM. The treated bacteria were incubated for 12 hours at 37°C. On completion of
546 treatment, resazurin was added to the bacteria at a final concentration of 1µg/ml, followed by
547 an incubation at 37°C, for 2 hours. Post incubation, fluorescence intensity was measured in
548 TECAN plate reader (Ex-540nm/ Em-590nm). Percentage viability was calculated by the
549 formula:

550 $$Percentage\ Viability = \frac{Treated\ Flourescence\ Intensity}{Untreated\ Flourescence\ Intensity} \times 100$$

551 **Griess assay for estimating extracellular NO production by macrophages on infection:**
552 Griess assay detects the presence of nitrite, a stable product of NO breakdown. The protocol
553 for the assay was adapted from [27], [79]. Briefly, 50µl of culture supernatants of infected
554 macrophages or sodium nitrite standards (0.6, 1.2, 2.4, 4.8, 9.7, 19.5, 39, 78.1 and 156.2 µM)

555 were treated with 50µl of 1% sulphanilamide (prepared in 5% phosphoric acid) and 50µl of
556 0.1% NED (N-1-naphthyl ethylene diamine dihydrochloride), followed by an incubation for
557 10 minutes at room temperature in the dark. On the appearance of a pink-purple colour product
558 absorbance was measured at 545 nm.

559 **Measurement of NO production in infected macrophages:** Intracellular NO production by
560 RAW264.7 cells upon infection was measured by staining with DAF-2DA. 16h post-infection
561 cells were treated with 5µM DAF-2DA and incubated for 30 minutes at 37°C. The cells were
562 washed with 1xPBS and acquired in BD FACSverse flow cytometer (Ex-491nm/ Em-513nm).

563 **Immunofluorescence microscopy for nitrotyrosine residues, NOD1 and NOD2:**
564 RAW264.7 cells were seeded on coverslips and infected with eGFP-tagged strains [80]. The
565 cells were fixed with 3.5% paraformaldehyde (PFA) 16h post-infection. The sample was
566 stained with the rabbit-raised anti-nitrotyrosine or goat-raised anti-NOD1 or NOD2 antibody
567 at a dilution of 1:100 (in 2.5% BSA, 0.01% saponin) overnight at 4°C, followed by staining
568 with the corresponding secondary antibody tagged with a fluorophore at a dilution of 1:200 in
569 2.5% BSA, 0.01% saponin for one hour at room temperature. The antibodies used in this study
570 are listed in Table 3. The coverslips were mounted on glass slides and sealed with transparent
571 nail polish. The coverslips were imaged by using a Zeiss 880 microscope. Zeiss ZEN Black
572 2012 software was used to analyse the images. The formula used for calculating corrected total
573 cell fluorescence (CTCF) is as follows:

574 $$CTCF = Integrated\ density$$
575 $$- (area\ of\ cell \times mean\ flourescent\ intensity\ of\ background)$$

576 Table 3. List of antibodies

Sr. No.	Antibody	Catalogue No

1	Anti-Nitrotyrosine Antibody	AB5411 (Sigma-Aldrich)
2	NOD2 (P-18) Antibody	sc-23587 (SCBT)
3	NOD1 (E-14) Antibody	sc-22045 (SCBT)
4	Goat raised anti-rabbit tagged with Cyanine5	Jackson Laboratory
5	Donkey raised anti-goat tagged with TRITC	Jackson Laboratory
6	CD16/CD32 Monoclonal Antibody (93)	14-0161-82 (eBioscience)
7	CD86 (B7-2) Monoclonal Antibody (GL1), PE	12-0862-82 (eBioscience)

577

578 **ELISA for estimating Nitrotyrosine and TNF-α:** For the estimation of Nitrotyrosine, 16h
579 post-infection, RAW264.7 cells were washed with 1x PBS and pelleted at 500g for 5 minutes.
580 The cells were lysed with native lysis buffer (150 mM NaCl, 2 mM EDTA, 20 mM Tris, pH 8,
581 1% NP-40) at 4°C, with intermittent vortexing for 30 minutes, followed by centrifugation at
582 13,000 RPM for 15 minutes at 4°C. The protein concentration of the supernatant was estimated
583 using the Bradford Reagent (Bio-Rad). Equal volumes of the supernatant, normalised to protein
584 content, were applied to the pre-coated ELISA plates of the Nitrotyrosine ELISA kit (Abcam,
585 ab210603), and the ELISA was performed according to the manufacturer's protocol. To
586 evaluate levels of TNF-α, the spent medium was collected from infected RAW264.7 cells 16
587 hours post-infection and subjected to centrifugation at 13,000 RPM, 4°C, for 10 minutes. The
588 supernatant was added to the pre-coated TNF-α ELISA plates of the GENLISA Mouse TNF-α
589 ELISA kit (Krishgen BioSystems, KB2145), and the ELISA was performed according to the
590 manufacturer's protocol. The final absorbance was measured at 450 nm wavelength using a
591 Tecan Plate reader, and the concentrations of Nitrotyrosine and TNF-α were interpolated from
592 a standard curve.

593 **Flow cytometry for assessing macrophage cell surface markers:** The protocol was adapted
594 from [81] and is as follows: Infected RAW 264.7 cells were washed and harvested in 1x PBS,

595 16 hours post-infection. Cells were centrifuged at 500g at 4°C, and the pellet was resuspended
596 in Fc blocking solution, comprising anti-mouse CD16/CD32 antibody at a dilution of 1:200 in
597 FACS buffer (1% BSA, 2 mM EDTA in 1x PBS), followed by a 30-minute incubation on ice.
598 Post-incubation, the cells were washed and stained with a PE-conjugated CD86 antibody at a
599 dilution of 1:200 for 1 hour on ice. Subsequently, the cells were washed and fixed with 2% PFA
600 in PBS for 10 minutes. The cells were washed with 1x PBS, resuspended in FACS buffer, and
601 acquired using CytoFLEX flow cytometer by Beckman Coulter Life Sciences. The data were
602 then analysed in CytExpert software.

603 **Bacterial burden in murine model:** Specific pathogen-free (SPF) 6-8 weeks old C57BL/6
604 (*iNOS*$^{+/+}$) and *iNos*$^{-/-}$ (*iNOS* knockout in C57BL/6 background) mice were segregated in
605 cohorts of n=5 or 6. For oral infection, C57BL/6 mice were orally gavaged with 10^7 CFU of
606 STM WT or STM*ΔuppP*. For *iNOS*$^{-/-}$ mice, a dose of 10^5 CFU was administered orally. The
607 infected mice were ethically euthanised 5 days post-infection. For intraperitoneal injection,
608 C57BL/6 (*iNOS*$^{+/+}$) and *iNOS*$^{-/-}$ mice were injected with a dose of 10^4 CFU, followed by ethical
609 euthanasia 3 days post-infection. Bacterial burden was enumerated in the homogenised lysate
610 of organs by serial dilution plating on *Salmonella-Shigella* agar.

611 **Mouse survival assay:** Specific pathogen-free (SPF) 6-8 weeks C57BL/6 mice were orally
612 gavaged with 10^7 CFU of STM WT or STM*ΔuppP* (n=6) and monitored daily for mortality.
613 The data is represented as survival percentage.

614 **Statistical analysis:** Data was analysed and graphed using the GraphPad Prism 8 software
615 (San Diego, CA). Statistical significance was determined by Student's t-test, One-way
616 ANOVA or Two-way ANOVA to obtain p values. Adjusted p-values below 0.05 are
617 considered statistically significant. The results are expressed as mean ± SD unless mentioned
618 otherwise.

Ethics statement

All the animal experiments have been approved by the Institutional Animal Ethics Clearance Committee (IAEC), Indian Institute of Science, Bangalore. The registration number is 48/1999/CPCSEA. The guidelines formulated by the Committee for the Purpose of Control and Supervision of Experiments on Animals (CPCSEA) were strictly followed. The ethical clearance number for this study is CAF/Ethics/853/2021.

Funding Information

We sincerely appreciate the financial support provided by the Department of Biotechnology (DBT) and the Department of Science and Technology (DST) from the Ministry of Science and Technology. DC acknowledges the Department of Atomic Energy-Scientific Research Council (DAE-SRC) for the Outstanding Investigator Award and funds, ASTRA Chair Professorship, and TATA Innovation fellowship funds. The authors collectively acknowledge the DBT-IISc Partnership Program. We gratefully acknowledge the infrastructure support from the Indian Council of Medical Research (Centre for Advanced Study in Molecular Medicine), DST-FIST (Fund for Improvement of Science and Technology Infrastructure), and the University Grants Commission (special assistance). RV acknowledges the Council of Scientific and Industrial Research (CSIR) for the fellowship. DM and KP acknowledge the Ministry of Human Resource Development (MHRD) for the fellowship. The funders had no role in study design, data collection and analysis, decision to publish, or preparation of the manuscript.

Acknowledgements

We acknowledge the Real-Time Facility, Departmental Confocal Microscopy Facility and Central Instrumentation Facility, at the Department of Microbiology and Cell Biology (MCB), the Division of Biological Sciences Flow Cytometry Facility, the Atomic Force

Microscopy (AFM) Facility at the Department of Bioengineering (BE), Advanced Facility for Microscopy and Microanalysis (AFMM) and Central Animal Facility at the Indian Institute of Science (IISc). Mrs. Deepika and Mrs. Monisha are acknowledged for their help in acquiring Scanning Electron Microscopy (SEM) images and AFM images, respectively. We are grateful to Mr. Munish and Mrs. Navya for helping with the data acquisition for flow cytometry. We thank Mr. Arjun Suresh for his assistance with confocal microscopy image acquisition. Dr Abhilash Vijay Nair is acknowledged for providing us with the gene of interest for our study.

Author Contributions

Conceptualisation: RV, DM, KP, and DC; Methodology: RV, DM, KP, KCN (PG isolation and analysis); Investigation: RV, DM, KP, KCN (PG isolation and analysis); Data curation: RV, Formal analysis: RV, DM, KP, Fund acquisition: DC, MR (PG isolation and analysis) Project administration: RV and DC, Writing-original draft: RV, Editing and proofreading: RV, DM, KP, KCN, MR and DC, Supervision: DC.

References

[1] A. Fàbrega and J. Vila, "Salmonella enterica serovar Typhimurium skills to succeed in the host: Virulence and regulation," *Clin Microbiol Rev*, vol. 26, no. 2, pp. 308–341, 2013, doi: 10.1128/CMR.00066-12.

[2] R. G. Ferrari, D. K. A. Rosario, A. Cunha-Neto, S. B. Mano, E. E. S. Figueiredo, and C. A. Conte-Juniora, "Worldwide epidemiology of Salmonella serovars in animal-based foods: A meta-analysis," *Appl Environ Microbiol*, vol. 85, no. 14, Jul. 2019, doi: 10.1128/AEM.00591-19/SUPPL_FILE/AEM.00591-19-S0001.PDF.

[3] S. Issenhuth-Jeanjean *et al.*, "Supplement 2008–2010 (no. 48) to the White–Kauffmann–Le Minor scheme," *Res Microbiol*, vol. 165, no. 7, pp. 526–530, Sep. 2014, doi: 10.1016/J.RESMIC.2014.07.004.

[4] O. Gal-Mor, "Persistent infection and long-term carriage of typhoidal and nontyphoidal salmonellae," *Clin Microbiol Rev*, vol. 32, no. 1, Jan. 2019, doi: 10.1128/CMR.00088-18.

[5] J. D. Stanaway *et al.*, "The global burden of non-typhoidal salmonella invasive disease: a systematic analysis for the Global Burden of Disease Study 2017," *Lancet*

Infect Dis, vol. 19, no. 12, pp. 1312–1324, Dec. 2019, doi: 10.1016/S1473-3099(19)30418-9.

[6] "WHO bacterial priority pathogens list, 2024: Bacterial pathogens of public health importance to guide research, development and strategies to prevent and control antimicrobial resistance." Accessed: Apr. 14, 2025. [Online]. Available: https://www.who.int/publications/i/item/9789240093461

[7] WHO, "WHO bacterial priority pathogens list, 2024: Bacterial pathogens of public health importance to guide research, development and strategies to prevent and control antimicrobial resistance," *Bacterial pathogens of public health importance to guide research, development and strategies to prevent and control antimicrobial resistance*, p. 72, 2024, Accessed: Apr. 14, 2025. [Online]. Available: https://www.who.int/publications/i/item/9789240093461

[8] P. Garai, D. P. Gnanadhas, and D. Chakravortty, "Salmonella enterica serovars typhimurium and typhi as model organisms: Revealing paradigm of host-pathogen interactions," *Virulence*, vol. 3, no. 4, pp. 377–388, 2012, doi: 10.4161/viru.21087.

[9] S. Garde, P. K. Chodisetti, and M. Reddy, "Peptidoglycan: Structure, Synthesis, and Regulation," *EcoSal Plus*, vol. 9, no. 2, Dec. 2021, doi: 10.1128/ecosalplus.esp-0010-2020.

[10] G. Manat *et al.*, "Deciphering the metabolism of undecaprenyl-phosphate: The bacterial cell-wall unit carrier at the membrane frontier," in *Microbial Drug Resistance*, Mary Ann Liebert Inc., Jun. 2014, pp. 199–214. doi: 10.1089/mdr.2014.0035.

[11] S. Kumar, A. Mollo, D. Kahne, and N. Ruiz, "The Bacterial Cell Wall: From Lipid II Flipping to Polymerization," *Chem Rev*, vol. 122, no. 9, pp. 8884–8910, May 2022, doi: 10.1021/ACS.CHEMREV.1C00773/ASSET/IMAGES/LARGE/CR1C00773_0011.JPEG.

[12] S. Booth and R. J. Lewis, "Structural basis for the coordination of cell division with the synthesis of the bacterial cell envelope," *Protein Science*, vol. 28, no. 12, pp. 2042–2054, Dec. 2019, doi: 10.1002/PRO.3722;.

[13] K. Emami *et al.*, "RodA as the missing glycosyltransferase in Bacillus subtilis and antibiotic discovery for the peptidoglycan polymerase pathway," *Nature Microbiology 2017 2:3*, vol. 2, no. 3, pp. 16253-, Jan. 2017, doi: 10.1038/nmicrobiol.2016.253.

[14] A. Taguchi *et al.*, "FtsW is a peptidoglycan polymerase that is functional only in complex with its cognate penicillin-binding protein," *Nature Microbiology 2019 4:4*, vol. 4, no. 4, pp. 587–594, Jan. 2019, doi: 10.1038/s41564-018-0345-x.

[15] M. El Ghachi, A. Bouhss, D. Blanot, and D. Mengin-Lecreulx, "The bacA gene of Escherichia coli encodes an undecaprenyl pyrophosphate phosphatase activity,"

Journal of Biological Chemistry, vol. 279, no. 29, pp. 30106–30113, Jul. 2004, doi: 10.1074/jbc.M401701200.

[16] M. El Ghachi, A. Derbise, A. Bouhss, and D. Mengin-Lecreulx, "Identification of multiple genes encoding membrane proteins with undecaprenyl pyrophosphate phosphatase (UppP) activity in Escherichia coli," *Journal of Biological Chemistry*, vol. 280, no. 19, pp. 18689–18695, May 2005, doi: 10.1074/jbc.M412277200.

[17] L. D. Tatar, C. L. Marolda, A. N. Polischuk, D. van Leeuwen, and M. A. Valvano, "An Escherichia coli undecaprenyl-pyrophosphate phosphatase implicated in undecaprenyl phosphate recycling," *Microbiology (N Y)*, vol. 153, no. 8, pp. 2518–2529, Aug. 2007, doi: 10.1099/mic.0.2007/006312-0.

[18] B. D. Cain, P. J. Norton, W. Eubanks, H. S. Nick, and C. M. Allen, "Amplification of the bacA Gene Confers Bacitracin Resistance to Escherichia coli," 1993.

[19] A. F. Chalker *et al.*, "The bacA gene, which determines bacitracin susceptibility in Streptococcus pneumoniae and Staphylococcus aureus, is also required for virulence," 2000. [Online]. Available: www.tigr.org

[20] E. Gasiorowski *et al.*, "HupA, the main undecaprenyl pyrophosphate and phosphatidylglycerol phosphate phosphatase in Helicobacter pylori is essential for colonization of the stomach," *PLoS Pathog*, vol. 15, no. 9, 2019, doi: 10.1371/journal.ppat.1007972.

[21] L. Röse, S. H. E. Kaufmann, and S. Daugelat, "Involvement of Mycobacterium smegmatis undecaprenyl phosphokinase in biofilm and smegma formation," *Microbes Infect*, vol. 6, no. 11, pp. 965–971, Sep. 2004, doi: 10.1016/J.MICINF.2004.05.011.

[22] T. Geiger, M. Pazos, M. Lara-Tejero, W. Vollmer, and J. E. Galán, "Peptidoglycan editing by a specific ld-transpeptidase controls the muramidase-dependent secretion of typhoid toxin," *Nature Microbiology 2018 3:11*, vol. 3, no. 11, pp. 1243–1254, Sep. 2018, doi: 10.1038/s41564-018-0248-x.

[23] J. C. Quintela, M. A. De Pedro, P. Zöllner, G. Allmaier, and F. G. Del Portillo, "Peptidoglycan structure of Salmonella typhimurium growing within cultured mammalian cells," *Mol Microbiol*, vol. 23, no. 4, pp. 693–704, Feb. 1997, doi: 10.1046/J.1365-2958.1997.2561621.X;

[24] G. Rico-Pérez, A. Pezza, M. G. Pucciarelli, M. A. de Pedro, F. C. Soncini, and F. García-del Portillo, "A novel peptidoglycan D,L-endopeptidase induced by Salmonella inside eukaryotic cells contributes to virulence," *Mol Microbiol*, vol. 99, no. 3, pp. 546–556, Feb. 2016, doi: 10.1111/MMI.13248;

[25] S. B. Hernández *et al.*, "Peptidoglycan editing in non-proliferating intracellular Salmonella as source of interference with immune signaling," *PLoS Pathog*, vol. 18, no. 1, p. e1010241, Jan. 2022, doi: 10.1371/JOURNAL.PPAT.1010241.

[26] K. A. Datsenko and B. L. Wanner, “One-step inactivation of chromosomal genes in Escherichia coli K-12 using PCR products,” *Proc Natl Acad Sci U S A*, vol. 97, no. 12, pp. 6640–6645, Jun. 2000, doi: 10.1073/PNAS.120163297/ASSET/103C1B8D-D302-4337-8E67-9F9084156407/ASSETS/GRAPHIC/PQ1201632006.JPEG.

[27] A. R. Chowdhury, S. Sah, U. Varshney, and D. Chakravortty, “Salmonella Typhimurium outer membrane protein A (OmpA) renders protection from nitrosative stress of macrophages by maintaining the stability of bacterial outer membrane,” *PLoS Pathog*, vol. 18, no. 8, p. e1010708, Aug. 2022, doi: 10.1371/JOURNAL.PPAT.1010708.

[28] J. Delwick, T. Nikolaus, S. Erdogan, and M. Hensel, “Environmental regulation of Salmonella pathogenicity island 2 gene expression,” *Mol Microbiol*, vol. 31, no. 6, pp. 1759–1773, Apr. 1999, doi: 10.1046/J.1365-2958.1999.01312.X.

[29] M. A. Jorgenson and J. C. Bryant, “A genetic screen to identify factors affected by undecaprenyl phosphate recycling uncovers novel connections to morphogenesis in Escherichia coli,” *Mol Microbiol*, vol. 115, no. 2, pp. 191–207, Feb. 2021, doi: 10.1111/mmi.14609.

[30] M. A. Jorgenson, S. Kannan, M. E. Laubacher, and K. D. Young, “Dead-end intermediates in the enterobacterial common antigen pathway induce morphological defects in Escherichia coli by competing for undecaprenyl phosphate,” *Mol Microbiol*, vol. 100, no. 1, pp. 1–14, Apr. 2016, doi: 10.1111/mmi.13284.

[31] M. A. Jorgenson and K. D. Young, “Interrupting biosynthesis of O antigen or the lipopolysaccharide core produces morphological defects in Escherichia coli by sequestering undecaprenyl phosphate,” *J Bacteriol*, vol. 198, no. 22, pp. 3070–3079, 2016, doi: 10.1128/JB.00550-16.

[32] E. R. Rojas *et al.*, “The outer membrane is an essential load-bearing element in Gram-negative bacteria,” *Nature 2018 559:7715*, vol. 559, no. 7715, pp. 617–621, Jul. 2018, doi: 10.1038/s41586-018-0344-3.

[33] G. Wood *et al.*, “Salmonella injectisome penetration of macrophages triggers rapid translation of transcription factors and protection against cell death,” *bioRxiv*, p. 2023.07.21.550113, Jul. 2024, doi: 10.1101/2023.07.21.550113.

[34] D. Hersh, D. M. Monack, M. R. Smith, N. Ghori, S. Falkow, and A. Zychlinsky, “The Salmonella invasin SipB induces macrophage apoptosis by binding to caspase-1,” *Proc Natl Acad Sci U S A*, vol. 96, no. 5, pp. 2396–2401, Mar. 1999, doi: 10.1073/PNAS.96.5.2396/ASSET/F6D52141-9395-4E16-A419-3F95A9B47CA4/ASSETS/GRAPHIC/PQ0494845006.JPEG.

[35] Y. Zhang *et al.*, “Programmed cell death and Salmonella pathogenesis: an interactive overview,” *Front Microbiol*, vol. 14, p. 1333500, Jan. 2023, doi: 10.3389/FMICB.2023.1333500/BIBTEX.

[36] A. McIntosh *et al.*, “SipA activation of caspase-3 is a decisive mediator of host cell survival at early stages of Salmonella enterica serovar Typhimurium infection,” *Infect Immun*, vol. 85, no. 9, Sep. 2017, doi: 10.1128/IAI.00393-17/SUPPL_FILE/ZII999092114SM5.AVI.

[37] E. Jennings, T. L. M. Thurston, and D. W. Holden, “Salmonella SPI-2 Type III Secretion System Effectors: Molecular Mechanisms And Physiological Consequences,” *Cell Host Microbe*, vol. 22, no. 2, pp. 217–231, 2017, doi: 10.1016/j.chom.2017.07.009.

[38] D. Drecktrah *et al.*, “Dynamic Behavior of Salmonella-Induced Membrane Tubules in Epithelial Cells,” *Traffic*, vol. 9, no. 12, pp. 2117–2129, Dec. 2008, doi: 10.1111/J.1600-0854.2008.00830.X.

[39] C. A. Henard and A. Vázquez-Torres, “Nitric oxide and salmonella pathogenesis,” *Front Microbiol*, vol. 2, no. APR, p. 9906, Apr. 2011, doi: 10.3389/FMICB.2011.00084/BIBTEX.

[40] S. Chen *et al.*, “Macrophages in immunoregulation and therapeutics,” Dec. 01, 2023, *Springer Nature*. doi: 10.1038/s41392-023-01452-1.

[41] E. P. Garvey *et al.*, “1400W Is a Slow, Tight Binding, and Highly Selective Inhibitor of Inducible Nitric-oxide Synthase in Vitro and in Vivo,” *Journal of Biological Chemistry*, vol. 272, no. 8, pp. 4959–4963, Feb. 1997, doi: 10.1074/JBC.272.8.4959.

[42] S. Mukherjee, S. Karmakar, and S. P. S. Babu, “TLR2 and TLR4 mediated host immune responses in major infectious diseases: a review,” *The Brazilian Journal of Infectious Diseases*, vol. 20, no. 2, pp. 193–204, Mar. 2016, doi: 10.1016/J.BJID.2015.10.011.

[43] L. O. Moreira and D. S. Zamboni, “NOD1 and NOD2 signaling in infection and inflammation,” *Front Immunol*, vol. 3, no. NOV, p. 35118, Nov. 2012, doi: 10.3389/FIMMU.2012.00328/XML/NLM.

[44] S. Tötemeyer *et al.*, “IFN-γ Enhances Production of Nitric Oxide from Macrophages via a Mechanism That Depends on Nucleotide Oligomerization Domain-2,” *The Journal of Immunology*, vol. 176, no. 8, pp. 4804–4810, Apr. 2006, doi: 10.4049/JIMMUNOL.176.8.4804.

[45] S. Thoma-Uszynski *et al.*, “Induction of direct antimicrobial activity through mammalian toll-like receptors,” *Science (1979)*, vol. 291, no. 5508, pp. 1544–1547, Feb. 2001, doi: 10.1126/SCIENCE.291.5508.1544/ASSET/AF8C5909-6776-4874-9ADC-0D81695FA094/ASSETS/GRAPHIC/SE0619197003.JPEG.

[46] Y. Lu *et al.*, “Palmitoylation of NOD1 and NOD2 is required for bacterial sensing,” *Science (1979)*, vol. 366, no. 6464, pp. 460–467, Oct. 2019, doi: 10.1126/SCIENCE.AAU6391/SUPPL_FILE/AAU6391-LU-SM.PDF.

[47] N. Nakamura *et al.*, “Endosomes are specialized platforms for bacterial sensing and NOD2 signalling,” *Nature 2014 509:7499*, vol. 509, no. 7499, pp. 240–244, Mar. 2014, doi: 10.1038/nature13133.

[48] P. Mistry *et al.*, “Inhibition of TLR2 signaling by small molecule inhibitors targeting a pocket within the TLR2 TIR domain,” *Proc Natl Acad Sci U S A*, vol. 112, no. 17, pp. 5455–5460, Apr. 2015, doi: 10.1073/pnas.1422576112.

[49] N. Matsunaga, N. Tsuchimori, T. Matsumoto, and M. Ii, “TAK-242 (resatorvid), a small-molecule inhibitor of Toll-like receptor (TLR) 4 signaling, binds selectively to TLR4 and interferes with interactions between TLR4 and its adaptor molecules,” *Mol Pharmacol*, vol. 79, no. 1, pp. 34–41, Jan. 2011, doi: 10.1124/mol.110.068064.

[50] U. Nachbur *et al.*, “A RIPK2 inhibitor delays NOD signalling events yet prevents inflammatory cytokine production,” *Nature Communications 2015 6:1*, vol. 6, no. 1, pp. 1–13, Mar. 2015, doi: 10.1038/ncomms7442.

[51] M. Jin *et al.*, “EGFR-MEK1/2 cascade negatively regulates bactericidal function of bone marrow macrophages in mice with Staphylococcus aureus osteomyelitis,” *PLoS Pathog*, vol. 20, no. 8 August, Aug. 2024, doi: 10.1371/journal.ppat.1012437.

[52] M. Schaechter, O. MaalØe, and N. O. Kjeldgaard, “Dependency on Medium and Temperature of Cell Size and Chemical Composition during Balanced Growth of Salmonella typhimurium,” *Microbiology (N Y)*, vol. 19, no. 3, pp. 592–606, Dec. 1958, doi: 10.1099/00221287-19-3-592.

[53] H. Bremer and P. P. Dennis, “Modulation of Chemical Composition and Other Parameters of the Cell at Different Exponential Growth Rates,” *EcoSal Plus*, vol. 3, no. 1, Jan. 2008, doi: 10.1128/ECOSAL.5.2.3/ASSET/EC65E8C7-8572-4870-BAE2-75BD45F44790/ASSETS/GRAPHIC/FIG3.GIF.

[54] M. G. Sargent, “Control of cell length in Bacillus subtilis,” *J Bacteriol*, vol. 123, no. 1, pp. 7–19, Jul. 1975, doi: 10.1128/JB.123.1.7-19.1975.

[55] S. Vadia and P. A. Levin, “Growth rate and cell size: a re-examination of the growth law,” *Curr Opin Microbiol*, vol. 24, pp. 96–103, Apr. 2015, doi: 10.1016/J.MIB.2015.01.011.

[56] L. K. Harris and J. A. Theriot, “Surface Area to Volume Ratio: A Natural Variable for Bacterial Morphogenesis,” *Trends Microbiol*, vol. 26, no. 10, pp. 815–832, Oct. 2018, doi: 10.1016/J.TIM.2018.04.008.

[57] L. K. Harris and J. A. Theriot, “Relative Rates of Surface and Volume Synthesis Set Bacterial Cell Size,” *Cell*, vol. 165, no. 6, pp. 1479–1492, Jun. 2016, doi: 10.1016/J.CELL.2016.05.045.

[58] L. K. Sycuro *et al.*, “Peptidoglycan Crosslinking Relaxation Promotes Helicobacter pylori’s Helical Shape and Stomach Colonization,” *Cell*, vol. 141, no. 5, pp. 822–833, May 2010, doi: 10.1016/J.CELL.2010.03.046.

[59] E. Frirdich *et al.*, “Peptidoglycan-Modifying Enzyme Pgp1 Is Required for Helical Cell Shape and Pathogenicity Traits in Campylobacter jejuni,” *PLoS Pathog*, vol. 8, no. 3, p. e1002602, Mar. 2012, doi: 10.1371/JOURNAL.PPAT.1002602.

[60] E. Frirdich and E. C. Gaynor, “Peptidoglycan hydrolases, bacterial shape, and pathogenesis,” *Curr Opin Microbiol*, vol. 16, no. 6, pp. 767–778, Dec. 2013, doi: 10.1016/J.MIB.2013.09.005.

[61] S. S. Justice, D. A. Hunstad, P. C. Seed, and S. J. Hultgren, “Filamentation by Escherichia coli subverts innate defenses during urinary tract infection,” *Proc Natl Acad Sci U S A*, vol. 103, no. 52, pp. 19884–19889, Dec. 2006, doi: 10.1073/PNAS.0606329104;.

[62] D. Chakravortty, I. Hansen-Wester, and M. Hensel, “Salmonella pathogenicity island 2 mediates protection of intracellular Salmonella from reactive nitrogen intermediates,” *Journal of Experimental Medicine*, vol. 195, no. 9, pp. 1155–1166, 2002, doi: 10.1084/jem.20011547.

[63] D. Chakravortty and M. Hensel, “Inducible nitric oxide synthase and control of intracellular bacterial pathogens,” *Microbes Infect*, vol. 5, no. 7, pp. 621–627, Jun. 2003, doi: 10.1016/S1286-4579(03)00096-0.

[64] D. J. Philpott, M. T. Sorbara, S. J. Robertson, K. Croitoru, and S. E. Girardin, “NOD proteins: regulators of inflammation in health and disease,” *Nature Reviews Immunology 2013 14:1*, vol. 14, no. 1, pp. 9–23, Dec. 2013, doi: 10.1038/nri3565.

[65] K. Geddes *et al.*, “Nod1 and Nod2 regulation of inflammation in the Salmonella colitis model,” *Infect Immun*, vol. 78, no. 12, pp. 5107–5115, Dec. 2010, doi: 10.1128/IAI.00759-10.

[66] M. B. Landes, † Murugesan, V. S. Rajaram, H. Nguyen, and L. S. Schlesinger, “Role for NOD2 in Mycobacterium tuberculosis-induced iNOS expression and NO production in human macrophages,” *J Leukoc Biol*, vol. 97, no. 6, pp. 1111–1119, Jun. 2015, doi: 10.1189/JLB.3A1114-557R.

[67] K. Shimada *et al.*, “The NOD/RIP2 Pathway Is Essential for Host Defenses Against Chlamydophila pneumoniae Lung Infection,” *PLoS Pathog*, vol. 5, no. 4, p. e1000379, Apr. 2009, doi: 10.1371/JOURNAL.PPAT.1000379.

[68] G. K. Silva *et al.*, “Cutting Edge: Nucleotide-Binding Oligomerization Domain 1-Dependent Responses Account for Murine Resistance against Trypanosoma cruzi Infection,” *The Journal of Immunology*, vol. 184, no. 3, pp. 1148–1152, Feb. 2010, doi: 10.4049/JIMMUNOL.0902254.

[69] A. R. Chowdhury, D. Mukherjee, A. K. Singh, and D. Chakravortty, “Loss of outer membrane protein A (OmpA) impairs the survival of Salmonella Typhimurium by inducing membrane damage in the presence of ceftazidime and meropenem,” *Journal*

of Antimicrobial Chemotherapy, vol. 77, no. 12, pp. 3376–3389, Nov. 2022, doi: 10.1093/JAC/DKAC327.

[70] N. G. Coldham, M. Webber, M. J. Woodward, and L. J. V. Piddock, "A 96-well plate fluorescence assay for assessment of cellular permeability and active efflux in Salmonella enterica serovar Typhimurium and Escherichia coli," *Journal of Antimicrobial Chemotherapy*, vol. 65, no. 8, pp. 1655–1663, Aug. 2010, doi: 10.1093/JAC/DKQ169.

[71] S. K. Singh, L. Saisree, R. N. Amrutha, and M. Reddy, "Three redundant murein endopeptidases catalyse an essential cleavage step in peptidoglycan synthesis of Escherichia coli K12," *Mol Microbiol*, vol. 86, no. 5, pp. 1036–1051, Dec. 2012, doi: 10.1111/mmi.12058.

[72] K. C. Nallamotu, R. Bahadur, M. Kaul, and M. Reddy, "Peptidoglycan Remodeling by an L,D-Transpeptidase, LdtD during Cold Shock in Escherichia coli," *J Bacteriol*, vol. 205, no. 1, Jan. 2023, doi: 10.1128/jb.00382-22.

[73] B. Glauner, J. V. Holtje, and U. Schwarz, "The composition of the murein of Escherichia coli.," *Journal of Biological Chemistry*, vol. 263, no. 21, pp. 10088–10095, Jul. 1988, doi: 10.1016/S0021-9258(19)81481-3.

[74] S. Mahalakshmi, M. R. Sunayana, L. Saisree, and M. Reddy, "YciM is an essential gene required for regulation of lipopolysaccharide synthesis in Escherichia coli," *Mol Microbiol*, vol. 91, no. 1, pp. 145–157, Jan. 2014, doi: 10.1111/mmi.12452.

[75] A. Datey *et al.*, "Rewiring of one carbon metabolism in Salmonella serves as an excellent live vaccine against systemic salmonellosis," *Vaccine*, vol. 36, no. 50, pp. 7715–7727, Nov. 2018, doi: 10.1016/J.VACCINE.2018.10.079.

[76] A. V. Nair, A. Singh, R. S. Rajmani, and D. Chakravortty, "Salmonella Typhimurium employs spermidine to exert protection against ROS-mediated cytotoxicity and rewires host polyamine metabolism to ameliorate its survival in macrophages," *Redox Biol*, vol. 72, p. 103151, Jun. 2024, doi: 10.1016/J.REDOX.2024.103151.

[77] D. Mukherjee and D. Chakravortty, "A Tale of Twins: The Distinct Roles of Intracellular and Extracellular Formate in Regulating Flagellar and Pathogenicity Island-1 Genes in Salmonella Typhimurium," *bioRxiv*, p. 2024.01.30.577997, Nov. 2024, doi: 10.1101/2024.01.30.577997.

[78] S. Grille *et al.*, "Salmonella enterica serovar Typhimurium immunotherapy for B-cell lymphoma induces broad anti-tumour immunity with therapeutic effect," *Immunology*, vol. 143, no. 3, pp. 428–437, Nov. 2014, doi: 10.1111/IMM.12320.

[79] P. Das, A. Lahiri, A. Lahiri, and D. Chakravorthy, "Novel role of the nitrite transporter NirC in Salmonella pathogenesis: SPI2-dependent suppression of inducible nitric oxide synthase in activated macrophages," *Microbiology (N Y)*, vol. 155, no. 8, pp. 2476–2489, Aug. 2009, doi: 10.1099/MIC.0.029611-0/CITE/REFWORKS.

[80] R. H. Valdivia, A. E. Hromockyj, D. Monack, L. Ramakrishnan, and S. Falkow, "Applications for green fluorescent protein (GFP) in the study of hostpathogen interactions," *Gene*, vol. 173, no. 1, pp. 47–52, Jan. 1996, doi: 10.1016/0378-1119(95)00706-7.

[81] D. Hajra, R. S. Rajmani, A. D. Chaudhary, S. K. Gupta, and D. Chakravortty, "Salmonella-induced SIRT1 and SIRT3 are crucial for maintaining the metabolic switch in bacteria and host for successful pathogenesis," *Elife*, vol. 13, Dec. 2024, doi: 10.7554/eLife.93125.

Figure Legends

Main Figures

Figure 1. Loss of *uppP* affects the bacterial cell dimensions and strength

A-C) Growth kinetics of STM WT and STM Δ*uppP* by measuring optical density at 595nm (OD_{595nm}) in LB (Luria Bertani) broth (A), M9 minimal media (B), and acidic F-media (C). Data are representative of N=3, n=3 ± SD (standard deviation).

D) Representative scanning electron micrographs of STM WT, STM Δ*uppP* and STM Δ*uppP*:*uppP* logarithmic phase cells (1:100 dilution). Red and yellow arrows represent cells with increased and decreased length, respectively. Scale bar = 5µm

E) Quantification of the length of the logarithmic phase (1:100 dilution) bacterial cells captured in the SEM images (D). Data are representative of N=2, n≥50 ± SD (standard deviation). One-way ANOVA was performed to obtain the p-values. (****P ≤ 0.0001, ***P ≤ 0.001, **P ≤ 0.01, *P ≤ 0.05 ns- non-significant)

F) Representative atomic force images of STM WT, STM Δ*uppP* and STM Δ*uppP*:*uppP*.

G) Quantification of Young's modulus (MPa- Megapascal) of the bacterial cells captured in the AFM images. Data are representative of n≥30 ± SD (standard deviation). One-way ANOVA

960 was performed to obtain the p-values. (****P ≤ 0.0001, ***P ≤ 0.001, **P ≤ 0.01, *P ≤ 0.05
961 ns- non-significant)

962 **Figure 2. *uppP* facilitates *Salmonella* to withstand nitrite and peroxynitrite stress**

963 A) Fold proliferation of STM WT, STM Δ*uppP*, and STM Δ*uppP*:*uppP*, within RAW 264.7
964 macrophages (MOI=10). Results are mean of N=4, n=3 ± SEM (standard error of mean). One-
965 way ANOVA was performed to obtain the p-values. (****P ≤ 0.0001, ***P ≤ 0.001, **P ≤
966 0.01, *P ≤ 0.05 ns- non-significant)

967 B) Percentage viability of STM WT and STM *ΔuppP* in the presence of varying concentrations
968 of H_2O_2 measured by resazurin assay. Results are representative of N=2, n=4 ± SD. Two-way
969 ANOVA was performed to obtain the p-values. (****P ≤ 0.0001, ***P ≤ 0.001, **P ≤ 0.01, *P
970 ≤ 0.05 ns- non-significant)

971 C) Estimation of reactive oxygen species (ROS) levels in STM WT, STM *ΔuppP* and STM
972 Δ*uppP*:*uppP* by H_2DCFDA staining in the presence of varying concentrations of H_2O_2. Results
973 are representative of N=5, n=4 ± SD. Two-way ANOVA was performed to obtain the p-values.
974 (****P ≤ 0.0001, ***P ≤ 0.001, **P ≤ 0.01, *P ≤ 0.05 ns- non-significant)

975 D-E) Representative image (D) and percentage viability (E) of resazurin assay of STM WT and
976 STM Δ*uppP* in the presence of varying concentrations of $NaNO_2$ (*in vitro* nitrite stress). Results
977 are representative of N=3, n=3 ± SD. Two-way ANOVA was performed to obtain the p-values.
978 (****P ≤ 0.0001, ***P ≤ 0.001, **P ≤ 0.01, *P ≤ 0.05 ns- non-significant)

979 F-G) Representative image (F) and percentage viability (G) of resazurin assay of STM WT and
980 STM Δ*uppP* in the presence of varying concentrations of $NaNO_2$ + H_2O_2 (*in vitro* peroxynitrite
981 stress). Results are representative of N=2, n=4 ± SD. Two-way ANOVA was performed to
982 obtain the p-values. (****P ≤ 0.0001, ***P ≤ 0.001, **P ≤ 0.01, *P ≤ 0.05 ns- non-significant)

983 H-J) Estimation of nitric oxide in STM WT and STM Δ*uppP* by DAF_2DA staining in the
984 presence of varying concentrations of $NaNO_2$ by flow cytometry. Representative SSCA vs
985 DAF_2DA dot plots of STM WT and STM Δ*uppP* (H). Quantification of DAF_2DA positive
986 percentage population (I) and median fluorescence intensity (MFI) (J). Results are
987 representative of N=3, n=4 ± SD. Two-way ANOVA was performed to obtain the p-values.
988 (****P ≤ 0.0001, ***P ≤ 0.001, **P ≤ 0.01, *P ≤ 0.05 ns- non-significant)

989 **Figure 3. *uppP* sustains *Salmonella* survival in macrophages by countering host-induced**
990 **nitrosative stress**

991 A) Estimation of extracellular nitrite by Griess assay in culture supernatants of RAW264.7
992 cells, 16h post-infection with STM WT, STM Δ*uppP* and STM Δ*uppP:uppP*, MOI=10, N=3,
993 n=3 ± SD. One-way ANOVA was performed to obtain the p-values. (****P ≤ 0.0001, ***P ≤
994 0.001, **P ≤ 0.01, *P ≤ 0.05 ns- non-significant)

995 B-C) Estimation of nitric oxide in macrophages infected with mCherry-tagged STM WT and
996 STM Δ*uppP* at MOI=20 by DAF_2DA staining followed by flow cytometry. Representative
997 mCherry vs SSC-A, DAF_2DA vs SSC-A, dot plots and histograms of STM WT and STM
998 Δ*uppP* (B). Quantification of DAF_2DA median fluorescence intensity (MFI) of the mCherry-
999 positive population (C). Results are representative of N=3, n=4 ± SD. An unpaired two-tailed
1000 Student's t-test was performed to obtain the p-values. (****P ≤ 0.0001, ***P ≤ 0.001, **P ≤
1001 0.01, *P ≤ 0.05 ns- non-significant)

1002 D-F) Representative immunofluorescence images of RAW 264.7 cells infected with STM WT
1003 and STM Δ*uppP* for 16h, MOI=10, immunostained for nitrotyrosine (D). Quantification of
1004 corrected total cell fluorescence (CTCF) of nitrotyrosine in infected cells (E) and colocalisation
1005 of nitrotyrosine with bacteria (F). Results are representative of N=3, n≥50 ± SD. Unpaired two-

1006 tailed Student's t-test was performed to obtain the p-values. (****P ≤ 0.0001, ***P ≤ 0.001,
1007 **P ≤ 0.01, *P ≤ 0.05 ns- non-significant)

1008 G) Quantification of *Nos2* mRNA expression in RAW264.7 cells infected with STM WT and
1009 STM Δ*uppP* for 16h. Results are representative of N=2, n=3 ± SD. One-way ANOVA was
1010 performed to obtain the p-values. (****P ≤ 0.0001, ***P ≤ 0.001, **P ≤ 0.01, *P ≤ 0.05 ns-
1011 non-significant)

1012 **Figure 4. *uppP* counters nitrosative stress during systemic infection**

1013 A) Fold proliferation of STM WT and STM Δ*uppP* within RAW 264.7 macrophages on
1014 treatment with 1400W MOI=10. Results are representative of N=3, n=3 ± SD (standard
1015 deviation). One-way ANOVA was performed to obtain the p-values. (****P ≤ 0.0001, ***P ≤
1016 0.001, **P ≤ 0.01, *P ≤ 0.05 ns- non-significant)

1017 B) Schematic representation of the experimental protocol followed for intraperitoneal (I.P.) and
1018 infection, enumerating bacterial burden in tissues

1019 C-E) Enumeration of bacterial burden in the blood (C), liver (D), and spleen (E) on infection
1020 via intraperitoneal injection in C57BL/6 (*iNOS*$^{+/+}$) and *iNOS*$^{-/-}$ mice. Results are representative
1021 of N=2 n=7 ± SEM (standard deviation). Mann-Whitney test was performed to obtain the p
1022 values. (****P ≤ 0.0001, ***P ≤ 0.001, **P ≤ 0.01, *P ≤ 0.05 ns- non-significant)

1023 F) Fold proliferation of STM WT and STM Δ*uppP* within RAW 264.7 macrophages on
1024 treatment with WEHI-345 MOI=10. Results are representative of N=3, n=3 ± SD (standard
1025 deviation). One-way ANOVA was performed to obtain the p-values. (****P ≤ 0.0001, ***P ≤
1026 0.001, **P ≤ 0.01, *P ≤ 0.05 ns- non-significant)

1027 G-H) Representative immunofluorescence images of RAW 264.7 cells infected with STM WT
1028 and STM Δ*uppP* for 16h, MOI=10, immunostained for NOD2 (G). Quantification of corrected

1029 total cell fluorescence (CTCF) of NOD2 in infected cells (H). Results are representative of
1030 N=2, n≥50 ± SD. One-way ANOVA was performed to obtain the p-values. (****P ≤ 0.0001,
1031 ***P ≤ 0.001, **P ≤ 0.01, *P ≤ 0.05 ns- non-significant)

1032 I) Fold proliferation of STM WT and STM Δ*uppP* within RAW 264.7 macrophages on
1033 treatment with Nodinitib-1 and GSK717, MOI=10. Results are mean of N=3, n=3 ± SEM
1034 (standard error of mean). One-way ANOVA was performed to obtain the p-values. (****P ≤
1035 0.0001, ***P ≤ 0.001, **P ≤ 0.01, *P ≤ 0.05 ns- non-significant)

1036 **Figure 5. Graphical Abstract**

1037 Increased susceptibility of STM Δ*uppP* to host nitrosative stress is indicated by elevated NO
1038 levels in RAW 264.7 cells and a greater accumulation of nitrotyrosine residues on the mutant.
1039 The elevated NO levels may be due to activation of NOD receptors, which is one of the factors
1040 contributing to STM Δ*uppP*'s reduced fold proliferation in RAW 264.7 cells and attenuated
1041 survival in the mouse model. NO: Nitric oxide, ONO_2^-: Peroxynitrite, NOD: Nucleotide-
1042 binding oligomerisation domain-containing protein, GlcNac: N-acetylglucosamine, MurNac:
1043 N-Acetylmuramic acid. Created with BioRender.com

1044

1045 **Supplementary Figures**

1046 **Figure S1. Loss of *uppP* affects the bacterial cell dimensions**

1047 A) Representative scanning electron micrographs of STM WT and STM Δ*uppP* stationary
1048 phase cells. Red and yellow arrows represent cells with increased and decreased length,
1049 respectively. Scale bar = 5μm

1050 B) Quantification of the length of the stationary phase bacterial cells captured in the SEM
1051 images (A). Data are representative of N=2, n≥50 ± SD (standard deviation). An unpaired two-

1052 tailed Student's t-test was performed to obtain the p-values. (****P ≤ 0.0001, ***P ≤ 0.001,
1053 **P ≤ 0.01, *P ≤ 0.05 ns- non-significant)

1054 C) Representative scanning electron micrographs of STM WT, STM Δ*uppP* and STM
1055 Δ*uppP*:*uppP* logarithmic phase cells (1:1000 dilution). Red and yellow arrows represent cells
1056 with increased and decreased length, respectively. Scale bar = 5μm

1057 D) Quantification of the length of the logarithmic phase (1:1000 dilution) bacterial cells
1058 captured in the SEM images (C). Data are representative of N=2, n≥50 ± SD (standard
1059 deviation). One-way ANOVA was performed to obtain the p-values. (****P ≤ 0.0001, ***P ≤
1060 0.001, **P ≤ 0.01, *P ≤ 0.05 ns- non-significant)

1061 E) Representative atomic force micrographs of STM WT, STM Δ*uppP* and STM Δ*uppP*:*uppP*.
1062 A 20 x 20μm^2 area from each coverslip was selected for imaging.

1063 F) Measurement of outer membrane porosity of STM WT, STM Δ*uppP* and STM Δ*uppP*:*uppP*,
1064 in the stationary and logarithmic phase by bisbenzimide uptake assay. Data are representative
1065 of N=3, n=4 ± SD (standard deviation). Two-way ANOVA was performed to obtain the p-
1066 values. (****P ≤ 0.0001, ***P ≤ 0.001, **P ≤ 0.01, *P ≤ 0.05 ns- non-significant)

1067 **Figure S2. Peptidoglycan and LPS composition of STM Δ*uppP***

1068 A-B) HPLC chromatograms showing petidoglycan composition of STM WT and STM
1069 Δ*uppP* strains grown in Luria Bertani broth. Strains were grown till they reached the early
1070 logarithmic phase (OD_{600nm} ~1). Data are representative of N=2. The identities of the peaks,
1071 according to their mass, are represented in the table (C).

1072 C) Table summarising the identity of the muropeptide fragment peaks observed in HPLC
1073 chromatograms (A) and (B).

1074 D) Silver staining gel of LPS isolated from STM WT, STM Δ*uppP* and STM Δ*uppP*:*uppP*.
1075 Data are representative of N=2.

1076 **Figure S3. *uppP* facilitates the intracellular survival of *Salmonella* in macrophages**

1077 A) Percentage phagocytosis of STM WT, STM Δ*uppP*, and STM Δ*uppP:uppP*, within RAW
1078 264.7 macrophages (MOI=10). Results are mean of N=3, n=3 ± SEM (standard error of mean).
1079 One-way ANOVA was performed to obtain the p-values. (****P ≤ 0.0001, ***P ≤ 0.001, **P
1080 ≤ 0.01, *P ≤ 0.05 ns- non-significant)

1081 B-C) Percentage invasion (B) and fold proliferation (C) of STM WT, STM Δ*uppP* and STM
1082 Δ*uppP:uppP* within colorectal adenocarcinoma cell line Caco-2 (MOI=10). Results are mean
1083 of N=3, n=3 ± SEM (standard error of mean). An unpaired two-tailed student's t-test was
1084 performed to obtain the p-values. (****P ≤ 0.0001, ***P ≤ 0.001, **P ≤ 0.01, *P ≤ 0.05 ns-
1085 non-significant)

1086 D-E) Quantification of the expression of *hilA*, *prgH*, *invF* and *sipA* during logarithmic (E) and
1087 stationary (F) phase in STM WT and STM Δ*uppP* cultured in LB broth. Results are
1088 representative of N=2, n=3 ± SD. Two-way ANOVA was performed to obtain the p-values.
1089 (****P ≤ 0.0001, ***P ≤ 0.001, **P ≤ 0.01, *P ≤ 0.05 ns- non-significant)

1090 F) Cell viability assay of RAW 264.7 cells, 16h post-infection with STM WT, STM Δ*uppP*,
1091 and STM Δ*uppP:uppP*. Results are representative of N=2, n=3 ± SD. Two-way ANOVA was
1092 performed to obtain the p-values. (****P ≤ 0.0001, ***P ≤ 0.001, **P ≤ 0.01, *P ≤ 0.05 ns-
1093 non-significant)

1094 G) Quantification of the expression of *spiC* and *sifA* during the stationary phase in STM WT
1095 and STM Δ*uppP* cultured in LB broth. Results are representative of N=2, n=3 ± SD. Two-way
1096 ANOVA was performed to obtain the p-values. (****P ≤ 0.0001, ***P ≤ 0.001, **P ≤ 0.01, *P
1097 ≤ 0.05 ns- non-significant)

1098 H) Percentage viability of resazurin assay of STM WT, STM Δ*uppP* and STM Δ*uppP:uppP* in
1099 the presence of varying concentrations of $NaNO_2$ (*in vitro* nitrite stress). Results are
1100 representative of N=3, n=3 ± SD. Two-way ANOVA was performed to obtain the p-values.
1101 (****P ≤ 0.0001, ***P ≤ 0.001, **P ≤ 0.01, *P ≤ 0.05 ns- non-significant)

1102 **Figure S4. STM Δ*uppP* upregulates nitric oxide (NO) levels in RAW 264.7 cells**

1103 A-C) Alternative gating strategy for Fig. 3A-B. Estimation of NO in macrophages infected
1104 with mCherry-tagged STM WT and STM Δ*uppP* by DAF_2DA staining followed by flow
1105 cytometry. Representative DAF_2DA vs mCherry scatter plots of STM WT and STM Δ*uppP*
1106 (A). Quantification of mCherry- DAF_2DA double-positive percentage population (B) and
1107 DAF_2DA median fluorescence intensity (MFI) (C). Results are representative of N=3, n=4 ±
1108 SD. Unpaired two-tailed Student's t-test was performed to obtain the p-values. (****P ≤
1109 0.0001, ***P ≤ 0.001, **P ≤ 0.01, *P ≤ 0.05 ns- non-significant)

1110 D-E) Estimation of NO, 16h post-infection with STM WT, STM Δ*uppP* and STM Δ*uppP:uppP*
1111 in RAW264.7 cells by DAF_2DA staining followed by flow cytometry. Representative SSC-A
1112 vs DAF_2DA dot plots and Count vs DAF_2DA histogram plots of STM WT, STM Δ*uppP*, and
1113 STM Δ*uppP:uppP* infected RAW 264.7 cells (D). Quantification of median fluorescence
1114 intensity (MFI) of DAF_2DA-positive population (E). Results are representative of N=2, n=4 ±
1115 SD. One-way ANOVA was performed to obtain the p-values. (****P ≤ 0.0001, ***P ≤ 0.001,
1116 **P ≤ 0.01, *P ≤ 0.05 ns- non-significant)

1117 F) Estimation of nitrotyrosine through ELISA, in cell lysates of RAW 264.7 cells infected with
1118 STM WT, STM *ΔuppP*, and STM Δ*uppP:uppP*. Results are representative of N=2, n=2 ± SD.
1119 One-way ANOVA was performed to obtain the p-values. (****P ≤ 0.0001, ***P ≤ 0.001, **P
1120 ≤ 0.01, *P ≤ 0.05 ns- non-significant)

1121 **Figure S5. STM Δ*uppP* triggers an enhanced immune response in RAW 264.7 cells**

1122 A-B) Flow cytometric analysis of cell surface levels of CD86 in macrophages, 16h post-
1123 infection with STM WT, STM Δ*uppP* and STM Δ*uppP:uppP*. Representative Count vs CD86
1124 (PE) histogram plots and SSC-A vs CD86 (PE) dot plots of STM WT, STM Δ*uppP* and STM
1125 Δ*uppP:uppP* infected RAW 264.7 cells (A). Quantification of median fluorescence intensity
1126 (MFI) of CD86 (PE) positive population (B). Results are representative of N=2, n=4 ± SD.
1127 One-way ANOVA was performed to obtain the p-values. (****P ≤ 0.0001, ***P ≤ 0.001, **P
1128 ≤ 0.01, *P ≤ 0.05 ns- non-significant)

1129 C) Estimation of pro-inflammatory cytokine TNF-α production through ELISA in cell
1130 supernatants of RAW 264.7 macrophages infected with STM WT, STM Δ*uppP*, and STM
1131 Δ*uppP:uppP* for 16 hours. Results are mean of N=2, n=2 ± SEM (standard error of mean).
1132 One-way ANOVA was performed to obtain the p-values. (****P ≤ 0.0001, ***P ≤ 0.001, **P
1133 ≤ 0.01, *P ≤ 0.05 ns- non-significant)

1134 **Figure S6. UppP facilitates *Salmonella* survival in the *in vivo* murine model**

1135 A) Schematic representation of the experimental protocol followed for enumerating bacterial
1136 burden in tissues upon oral gavage in C57BL/6 ($iNOS^{+/+}$) mice.

1137 B-F) Enumeration of bacterial burden in the blood (B), intestine (C), MLN (D), spleen (E) and
1138 liver (F) on infection via oral route in C57BL/6 ($iNOS^{+/+}$) mice. Results are representative of
1139 N=2, n=6 ± SD (standard deviation). Mann-Whitney test was performed to obtain the p-values.
1140 (****P ≤ 0.0001, ***P ≤ 0.001, **P ≤ 0.01, *P ≤ 0.05 ns- non-significant)

1141 G) Percentage survival of C57BL/6 ($iNOS^{+/+}$) mice infected with STM WT and STMΔ*uppP*
1142 via the oral route.

1143 H) Schematic representation of the experimental protocol followed for enumerating bacterial
1144 burden in tissues upon oral gavage in *iNOS*$^{-/-}$ mice.

1145 I-M) Enumeration of bacterial burden in the blood (I), intestine (J), MLN (K), liver (L) and
1146 spleen (M) on infection via oral route in *iNOS*$^{-/-}$ mice. Results are representative of n=5 ± SD
1147 (standard deviation). Mann-Whitney test was performed to obtain the p-values. (****P ≤
1148 0.0001, ***P ≤ 0.001, **P ≤ 0.01, *P ≤ 0.05 ns- non-significant)

1149 **Figure S7. NOD receptors contribute to the attenuated survival of STM Δ*uppP* in RAW**
1150 **264.7 cells**

1151 A) Fold proliferation of STM WT and STM Δ*uppP* within RAW 264.7 macrophages on
1152 treatment with C29 and Resatorvid, MOI=10. Results are mean of N=3, n=3 ± SEM (standard
1153 error of mean). One-way ANOVA was performed to obtain the p-values. (****P ≤ 0.0001, ***P
1154 ≤ 0.001, **P ≤ 0.01, *P ≤ 0.05 ns- non-significant)

1155 B-C) Quantification of mRNA expression of *Nod1* (B) and *Nod2* (C) in RAW264.7 cells
1156 infected with STM WT and STM Δ*uppP* for 2h, 6h and 16h. Results are representative of N=3,
1157 n=3 ± SD. Two-way ANOVA was performed to obtain the p-values. (****P ≤ 0.0001, ***P ≤
1158 0.001, **P ≤ 0.01, *P ≤ 0.05 ns- non-significant)

1159 D-E) Representative immunofluorescence images of RAW 264.7 cells infected with STM WT
1160 and STM Δ*uppP* for 6h, MOI=10, immunostained for NOD1 (D). Quantification of corrected
1161 total cell fluorescence (CTCF) of NOD1 in infected cells (E). Results are representative of
1162 N=2, n≥50 ± SD. One-way ANOVA was performed to obtain the p-values. (****P ≤ 0.0001,
1163 ***P ≤ 0.001, **P ≤ 0.01, *P ≤ 0.05 ns- non-significant)

Figure 1

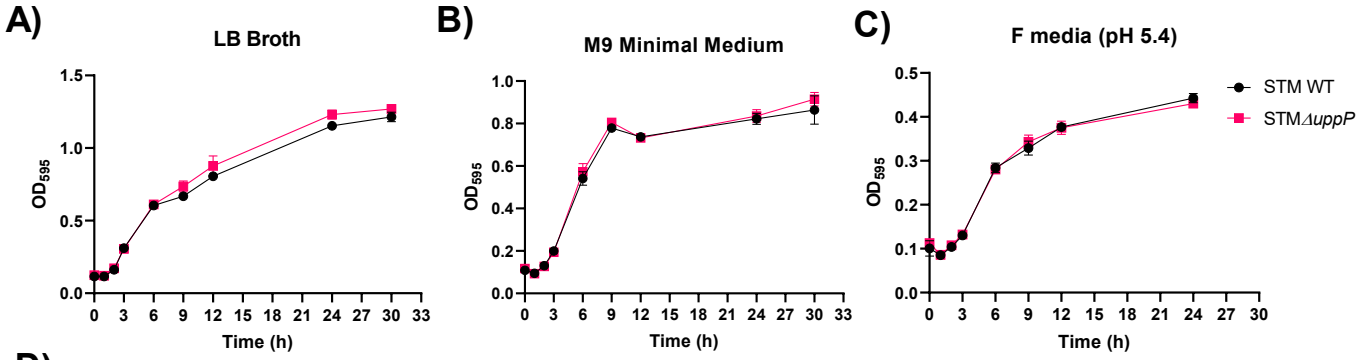
A)
LB Broth
B)
M9 Minimal Medium
C)
F media (pH 5.4)
STM WT
STMΔuppP
OD595
Time (h)

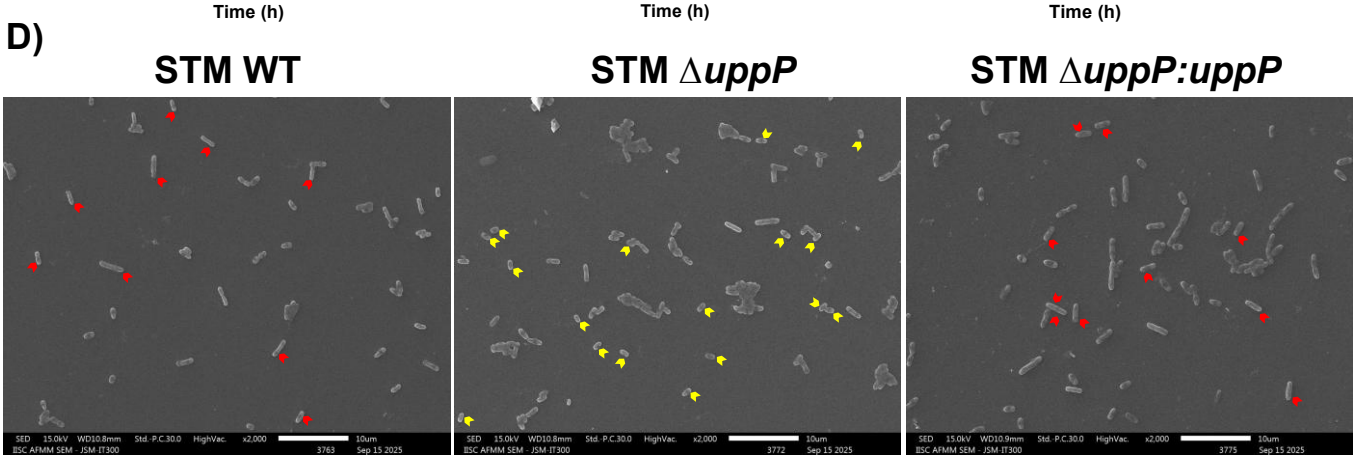
D)
STM WT
STM ΔuppP
STM ΔuppP:uppP

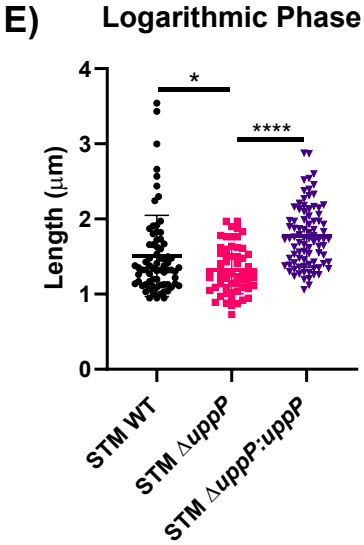
E)
Logarithmic Phase
Length (µm)
STM WT
STM ΔuppP
STM ΔuppP:uppP

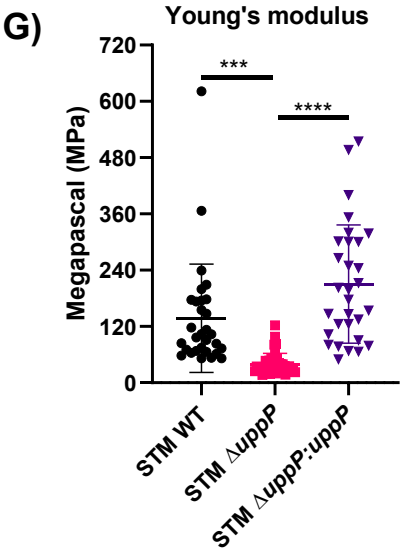
G)
Young's modulus
Megapascal (MPa)
STM WT
STM ΔuppP
STM ΔuppP:uppP

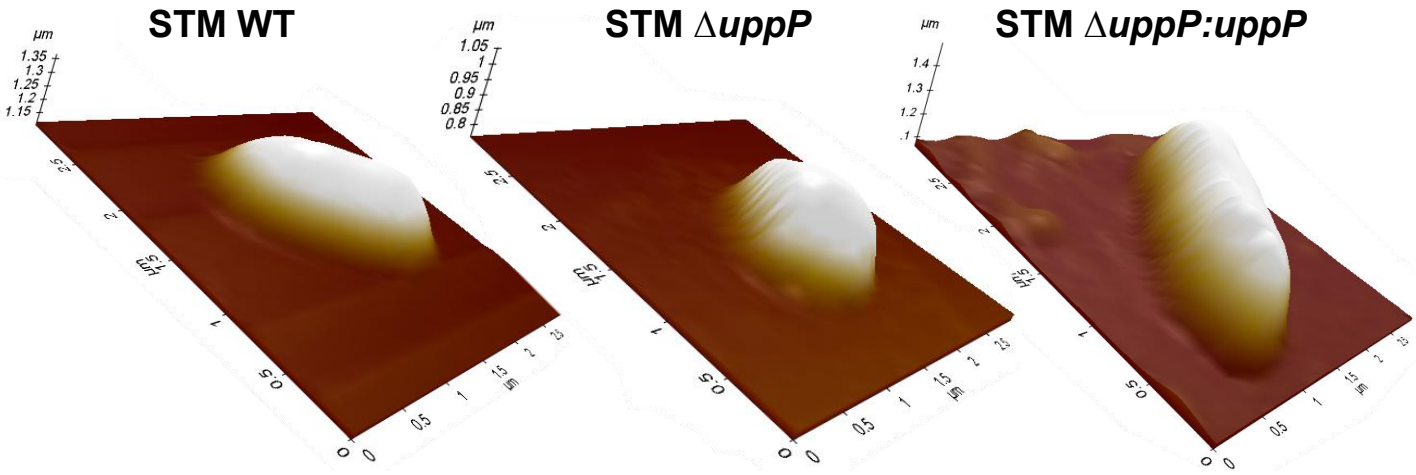
F)
STM WT
STM ΔuppP
STM ΔuppP:uppP

Figure 2

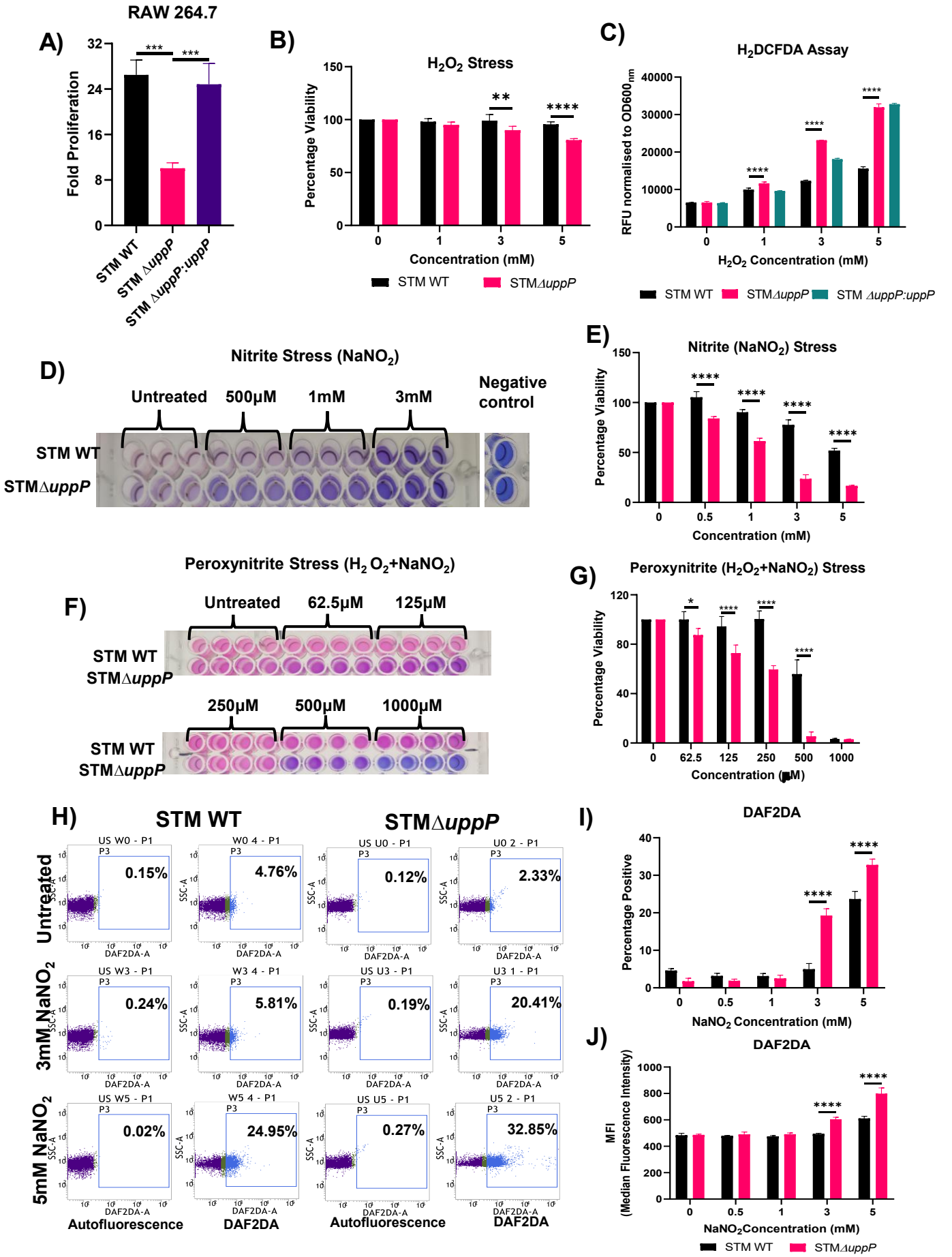
RAW 264.7
A)
Fold Proliferation
STM WT
STM ΔuppP
STM ΔuppP:uppP
B)
H2O2 Stress
Percentage Viability
Concentration (mM)
STM WT
STMΔuppP
C)
H2DCFDA Assay
RFU normalised to OD600nm
H2O2 Concentration (mM)
STM WT
STMΔuppP
STM ΔuppP:uppP
D)
Nitrite Stress (NaNO2)
Untreated
500µM
1mM
3mM
Negative control
STM WT
STMΔuppP
E)
Nitrite (NaNO2) Stress
Percentage Viability
Concentration (mM)
Peroxynitrite Stress (H2O2+NaNO2)
F)
Untreated
62.5µM
125µM
250µM
500µM
1000µM
STM WT
STMΔuppP
G)
Peroxynitrite (H2O2+NaNO2) Stress
Percentage Viability
Concentration (µM)
H)
STM WT
STMΔuppP
Untreated
3mM NaNO2
5mM NaNO2
0.15%
4.76%
0.12%
2.33%
0.24%
5.81%
0.19%
20.41%
0.02%
24.95%
0.27%
32.85%
Autofluorescence
DAF2DA
I)
DAF2DA
Percentage Positive
NaNO2 Concentration (mM)
J)
DAF2DA
MFI (Median Fluorescence Intensity)
NaNO2Concentration (mM)
STM WT
STMΔuppP

Figure 3

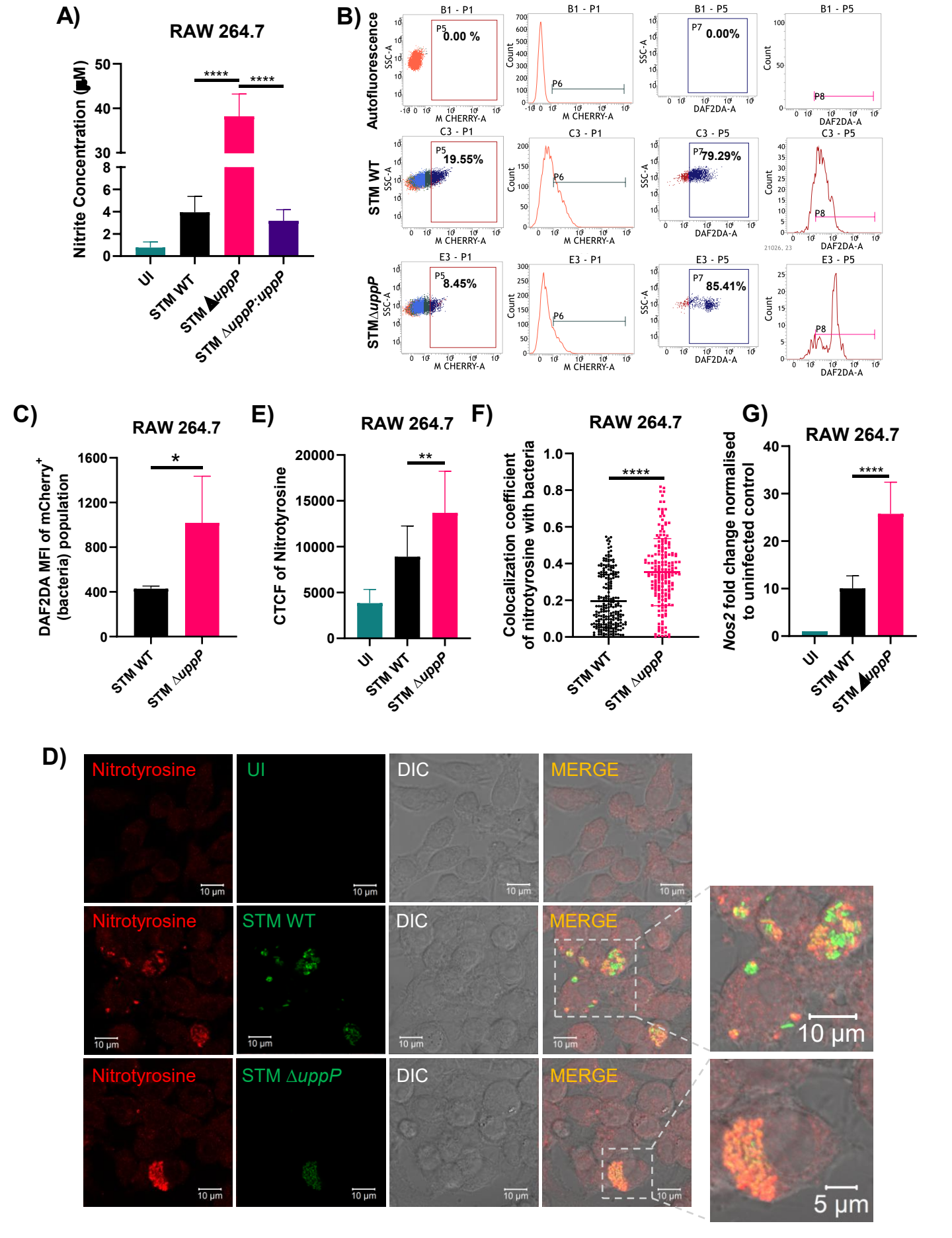
A)
RAW 264.7
Nitrite Concentration (μM)
****
****
UI
STM WT
STM ΔuppP
STM ΔuppP:uppP
B)
Autofluorescence
STM WT
STMΔuppP
B1 - P1
B1 - P5
C3 - P1
C3 - P5
E3 - P1
E3 - P5
P5 0.00 %
P7 0.00%
P5 19.55%
P7 79.29%
P5 8.45%
P7 85.41%
P6
P8
SSC-A
M CHERRY-A
DAF2DA-A
Count
C)
RAW 264.7
DAF2DA MFI of mCherry+ (bacteria) population
*
STM WT
STM ΔuppP
E)
RAW 264.7
CTCF of Nitrotyrosine
**
UI
STM WT
STM ΔuppP
F)
RAW 264.7
Colocalization coefficient of nitrotyrosine with bacteria
****
STM WT
STM ΔuppP
G)
RAW 264.7
Nos2 fold change normalised to uninfected control
****
UI
STM WT
STM ΔuppP
D)
Nitrotyrosine
UI
DIC
MERGE
STM WT
STM ΔuppP
10 μm
5 μm

Figure 4

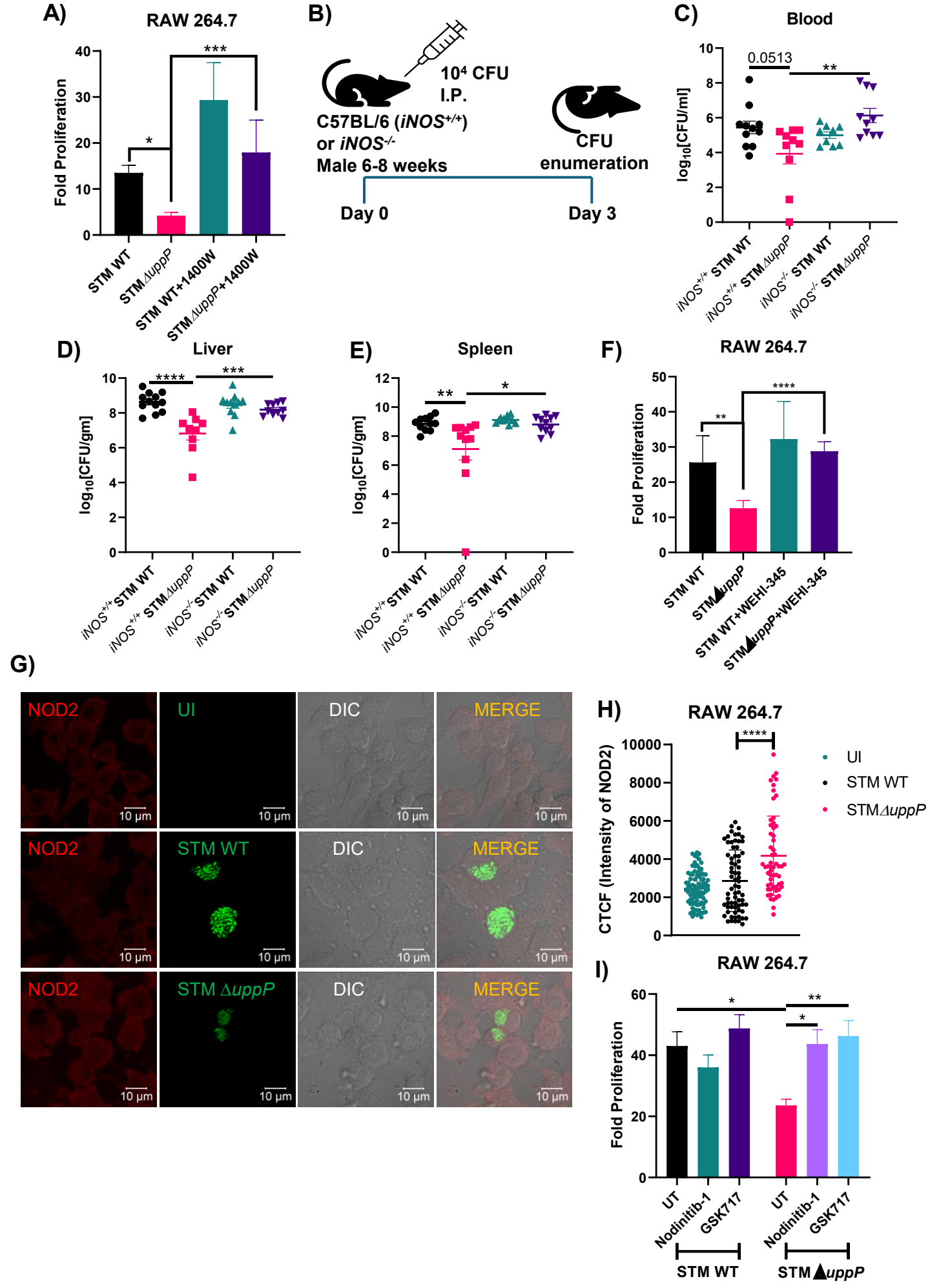
A)
RAW 264.7
Fold Proliferation
STM WT
STMΔuppP
STM WT+1400W
STMΔuppP+1400W
B)
10⁴ CFU
I.P.
C57BL/6 (iNOS+/+)
or iNOS-/-
Male 6-8 weeks
CFU
enumeration
Day 0
Day 3
C)
Blood
0.0513
log10[CFU/ml]
iNOS+/+ STM WT
iNOS+/+ STMΔuppP
iNOS-/- STM WT
iNOS-/- STMΔuppP
D)
Liver
log10[CFU/gm]
E)
Spleen
F)
RAW 264.7
STM WT+WEHI-345
STMΔuppP+WEHI-345
G)
NOD2
UI
DIC
MERGE
STM WT
STM ΔuppP
10 µm
H)
RAW 264.7
CTCF (Intensity of NOD2)
UI
STM WT
STMΔuppP
I)
RAW 264.7
Fold Proliferation
UT
Nodinitib-1
GSK717
STM WT
STMΔuppP

Graphical Summary

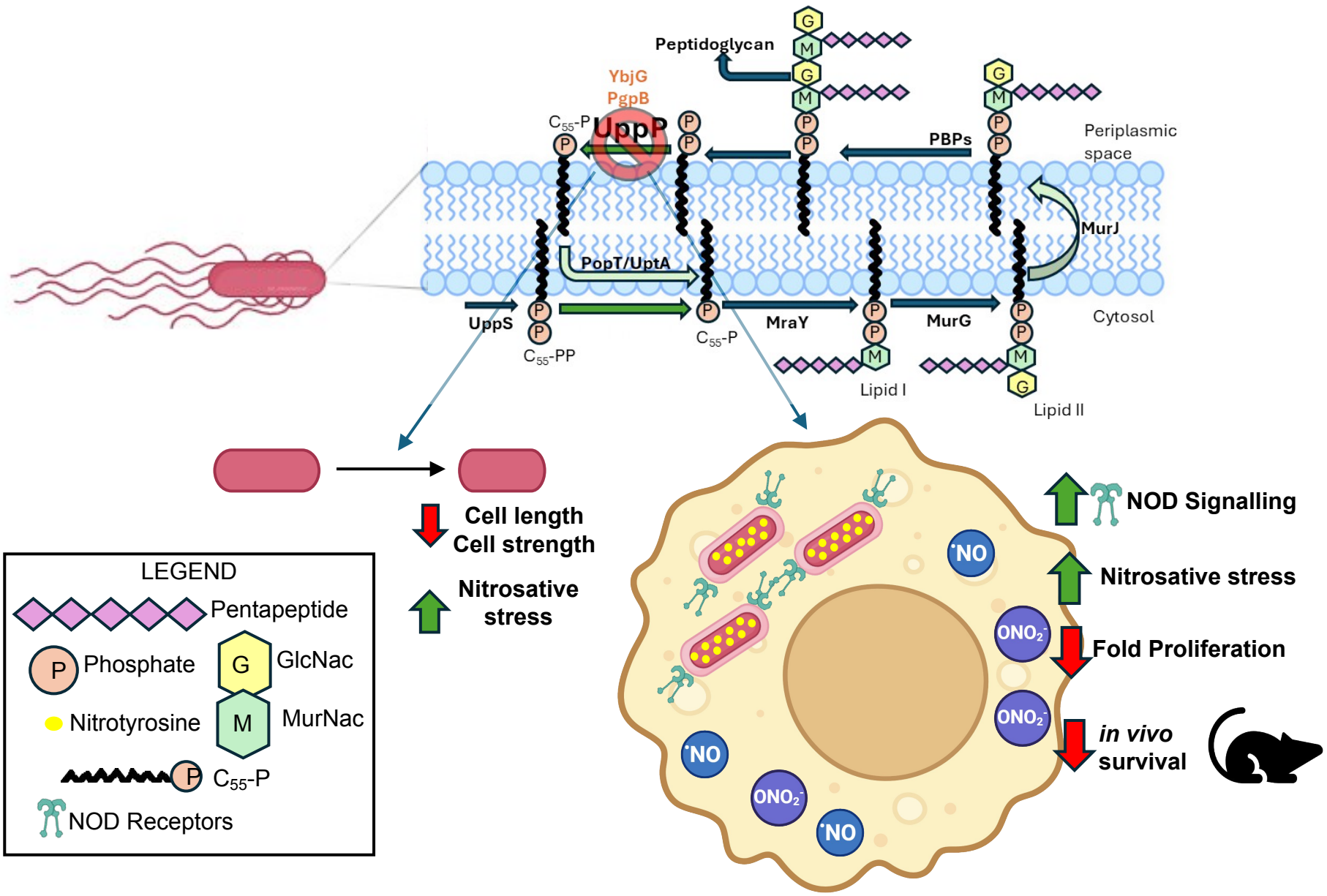

Figure S1

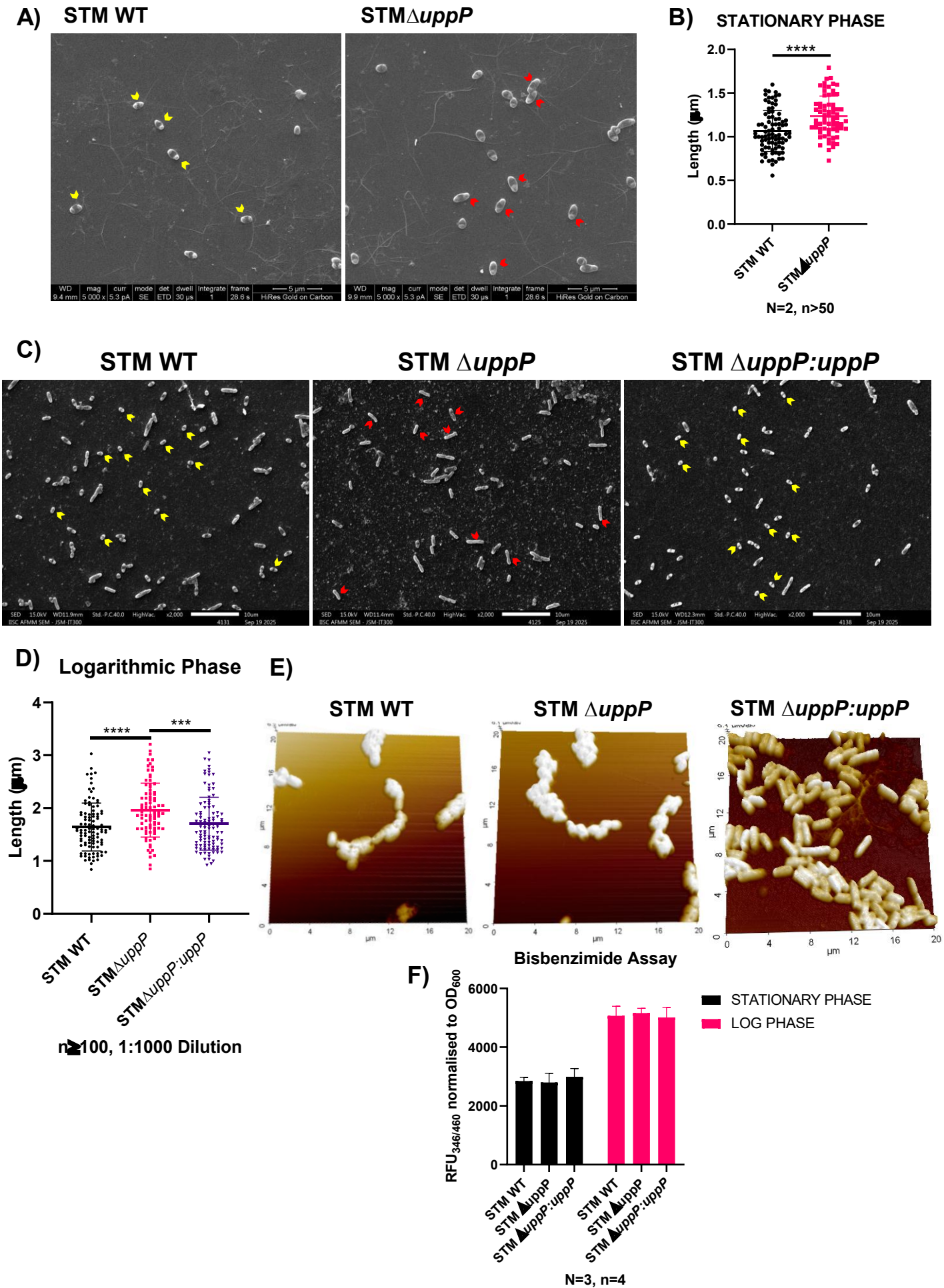
A)
STM WT
STMΔuppP
B)
STATIONARY PHASE
****
Length (µm)
2.0
1.5
1.0
0.5
0.0
STM WT
STMΔuppP
N=2, n>50
C)
STM WT
STM ΔuppP
STM ΔuppP:uppP
D)
Logarithmic Phase
****
***
Length (µm)
4
3
2
1
0
STM WT
STMΔuppP
STMΔuppP:uppP
n≥100, 1:1000 Dilution
E)
STM WT
STM ΔuppP
STM ΔuppP:uppP
µm
Bisbenzimide Assay
F)
RFU346/460 normalised to OD600
6000
4000
2000
0
STATIONARY PHASE
LOG PHASE
STM WT
STM ΔuppP
STM ΔuppP:uppP
N=3, n=4

Figure S2

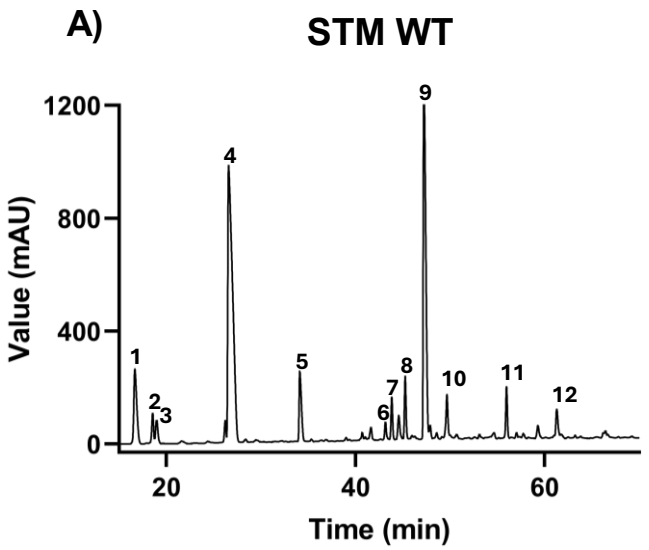

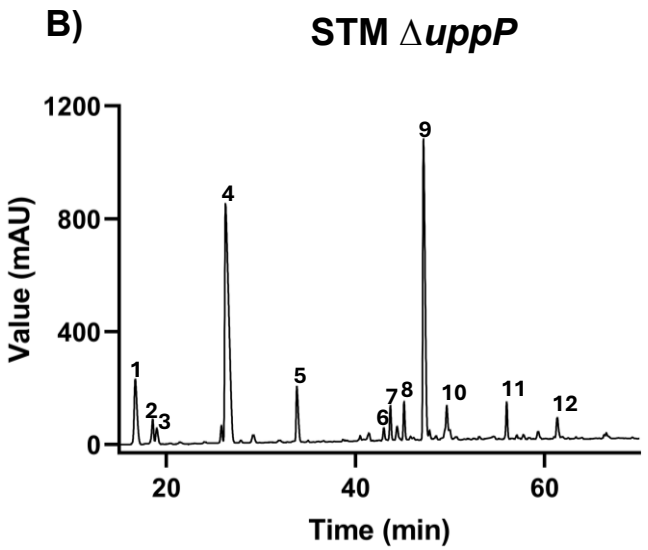

C)

Peak no	Muropeptide Species	Cross-link type
1	Tri	Un-crosslinked
2	Di	Un-crosslinked
3	Tetra(Gly^4)	Un-crosslinked with Glycine in 4th position
4	Terta	Un-crosslinked
5	Tri-lys-arg	Tri peptide bound to Braun's lipoprotein (Lpp)
6	Tri-Tri	3-3 cross-links
7	Tetra-Tri	4-3 cross-links
8	Tri-Tetra	3-3 cross-links
9	Tetra-Tetra	4-3 cross-links
10	Tetra-Tri-lys-arg	4-3 cross linked muropeptide bound to Lpp
11	Tetra-Tetra-Tetra	4-3 cross-links
12	Tetra-Tetra-Anh	4-3 cross-links

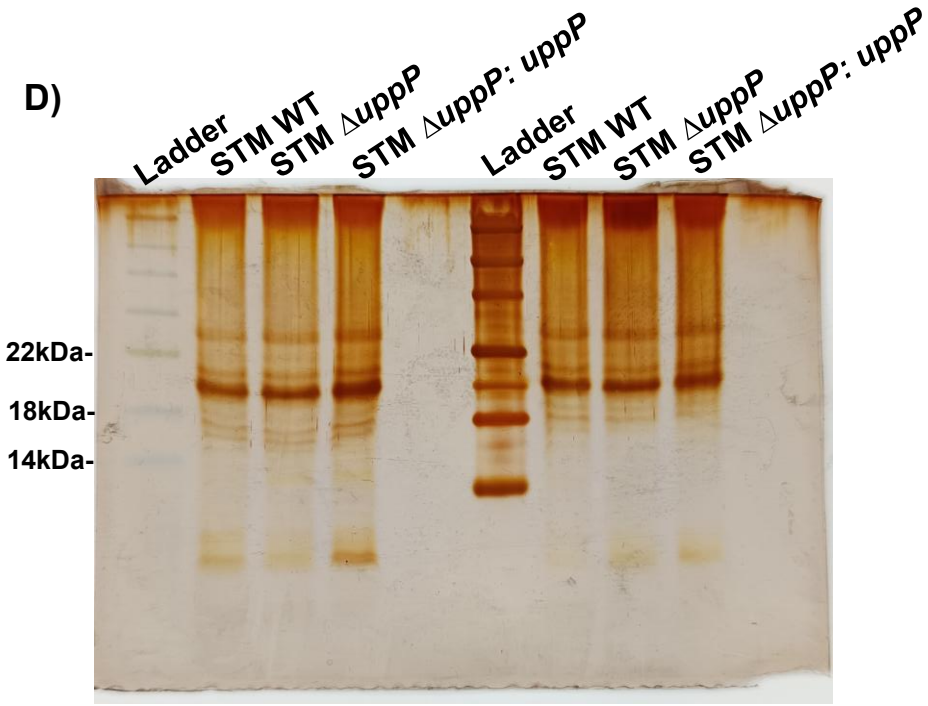

Figure S3

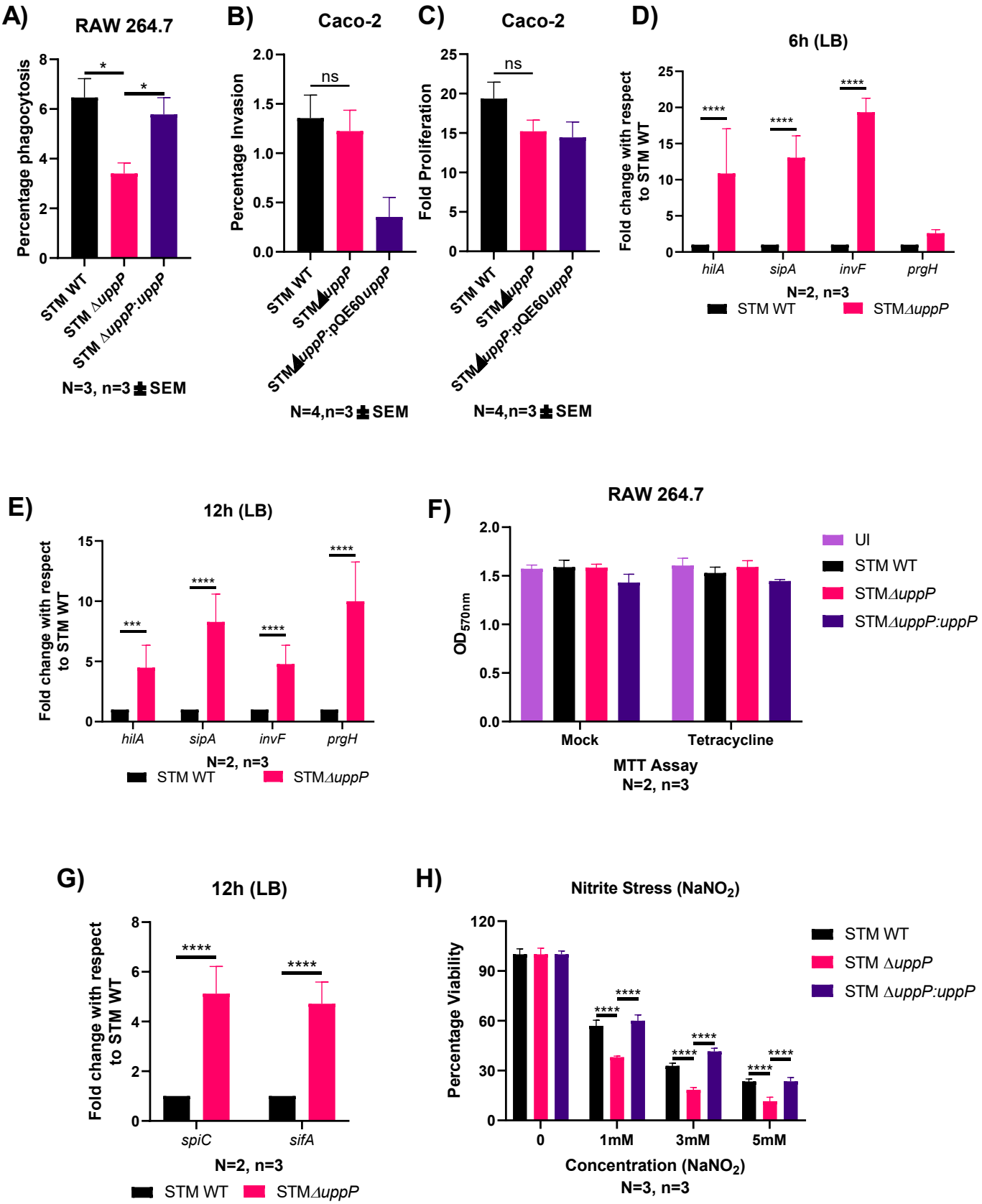
A)
RAW 264.7
Percentage phagocytosis
STM WT
STM ΔuppP
STM ΔuppP:uppP
N=3, n=3 ± SEM
B)
Caco-2
Percentage Invasion
ns
STM WT
STM ΔuppP
STM ΔuppP:pQE60uppP
N=4,n=3 ± SEM
C)
Caco-2
Fold Proliferation
ns
STM WT
STM ΔuppP
STM ΔuppP:pQE60uppP
N=4,n=3 ± SEM
D)
6h (LB)
Fold change with respect to STM WT
hilA
sipA
invF
prgH
N=2, n=3
STM WT
STMΔuppP
E)
12h (LB)
Fold change with respect to STM WT
hilA
sipA
invF
prgH
N=2, n=3
STM WT
STMΔuppP
F)
RAW 264.7
OD570nm
UI
STM WT
STMΔuppP
STMΔuppP:uppP
Mock
Tetracycline
MTT Assay
N=2, n=3
G)
12h (LB)
Fold change with respect to STM WT
spiC
sifA
N=2, n=3
STM WT
STMΔuppP
H)
Nitrite Stress (NaNO2)
Percentage Viability
STM WT
STM ΔuppP
STM ΔuppP:uppP
0
1mM
3mM
5mM
Concentration (NaNO2)
N=3, n=3

Figure S4

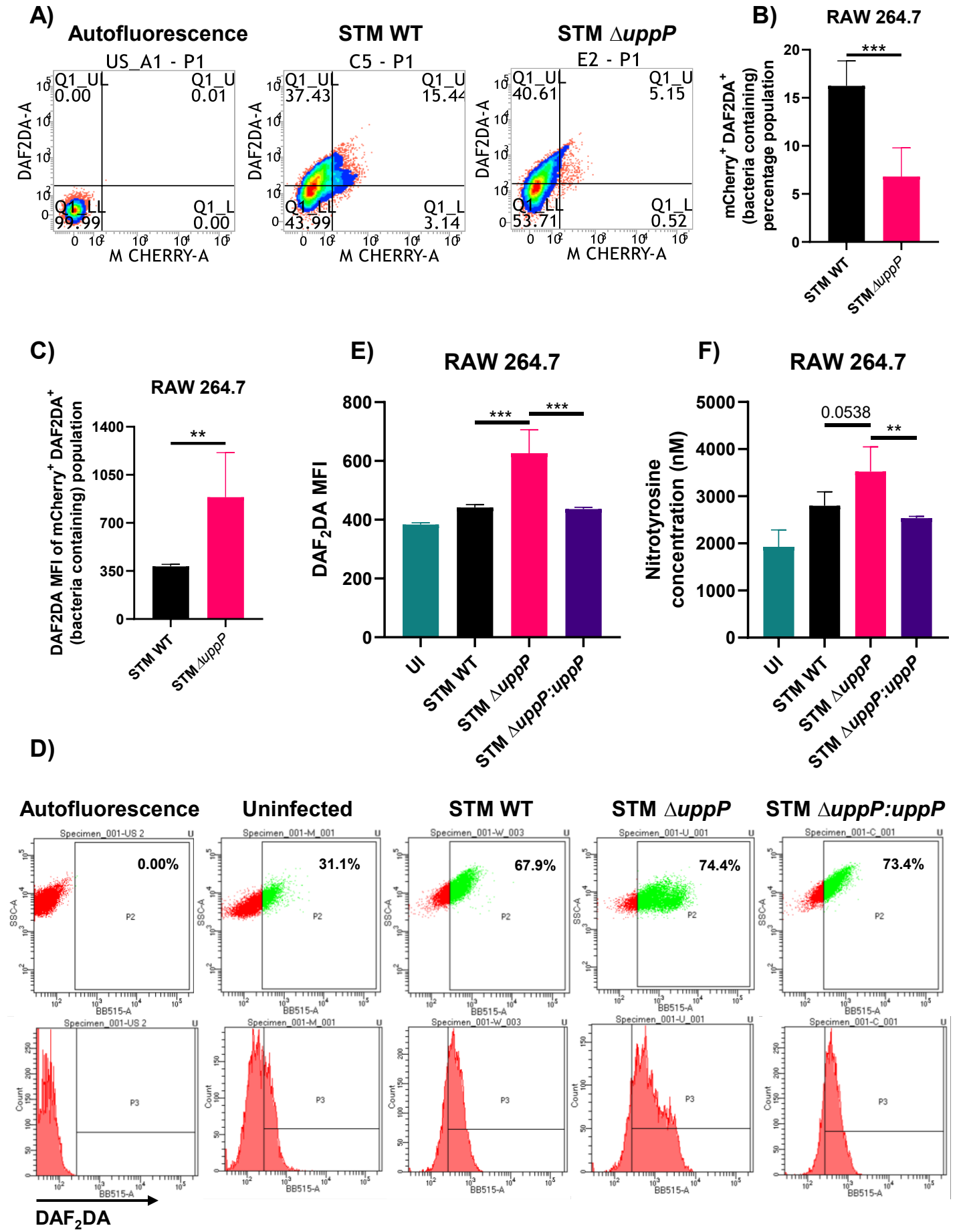
A)
Autofluorescence
STM WT
STM ΔuppP
US_A1 - P1
C5 - P1
E2 - P1
Q1_UL 0.00
Q1_U 0.01
Q1_LL 99.99
Q1_L 0.00
Q1_UL 37.43
Q1_U 15.44
Q1_LL 43.99
Q1_L 3.14
Q1_UL 40.61
Q1_U 5.15
Q1_LL 53.71
Q1_L 0.52
DAF2DA-A
M CHERRY-A
B)
RAW 264.7
mCherry+ DAF2DA+ (bacteria containing) percentage population
***
STM WT
STMΔuppP
C)
RAW 264.7
DAF2DA MFI of mCherry+ DAF2DA+ (bacteria containing) population
**
STM WT
STMΔuppP
E)
RAW 264.7
DAF2DA MFI
***
***
UI
STM WT
STM ΔuppP
STM ΔuppP:uppP
F)
RAW 264.7
Nitrotyrosine concentration (nM)
0.0538
**
UI
STM WT
STM ΔuppP
STM ΔuppP:uppP
D)
Autofluorescence
Uninfected
STM WT
STM ΔuppP
STM ΔuppP:uppP
0.00%
31.1%
67.9%
74.4%
73.4%
SSC-A
BB515-A
Count
DAF2DA

Figure S5

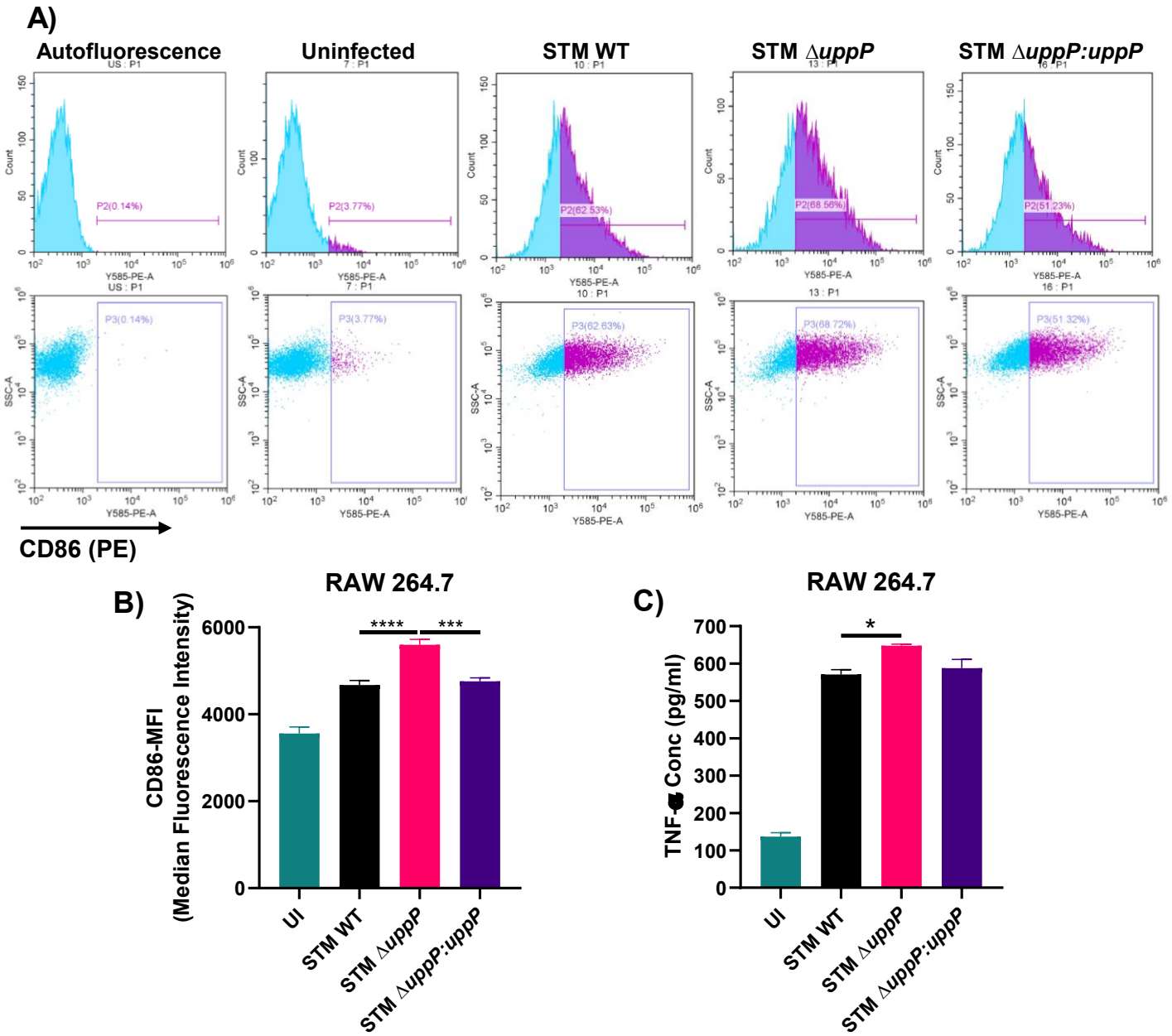
A)
Autofluorescence
Uninfected
STM WT
STM ΔuppP
STM ΔuppP:uppP
P2(0.14%)
P2(3.77%)
P2(62.53%)
P2(68.56%)
P2(51.23%)
P3(0.14%)
P3(3.77%)
P3(62.63%)
P3(68.72%)
P3(51.32%)
Count
SSC-A
Y585-PE-A
CD86 (PE)
B)
RAW 264.7
CD86-MFI
(Median Fluorescence Intensity)
****
***
UI
STM WT
STM ΔuppP
STM ΔuppP:uppP
C)
RAW 264.7
TNF-α Conc (pg/ml)
*

Figure S6

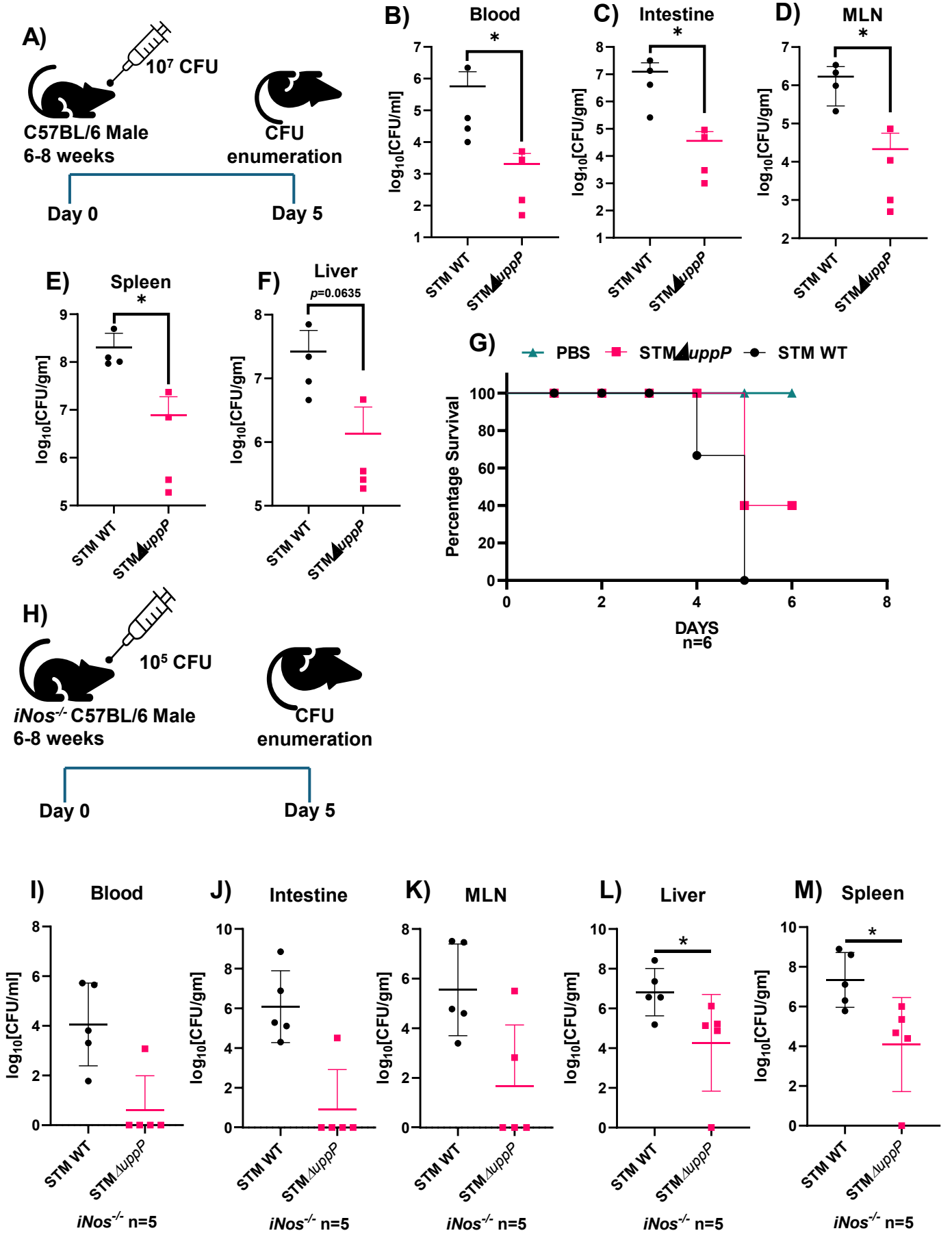
A)
10^7 CFU
C57BL/6 Male
6-8 weeks
CFU
enumeration
Day 0
Day 5
B) Blood
C) Intestine
D) MLN
E) Spleen
F) Liver
p=0.0635
log10[CFU/ml]
log10[CFU/gm]
STM WT
STMΔuppP
G)
PBS
STMΔuppP
STM WT
Percentage Survival
DAYS
n=6
H)
10^5 CFU
iNos-/- C57BL/6 Male
6-8 weeks
CFU
enumeration
Day 0
Day 5
I) Blood
J) Intestine
K) MLN
L) Liver
M) Spleen
iNos-/- n=5

Figure S7

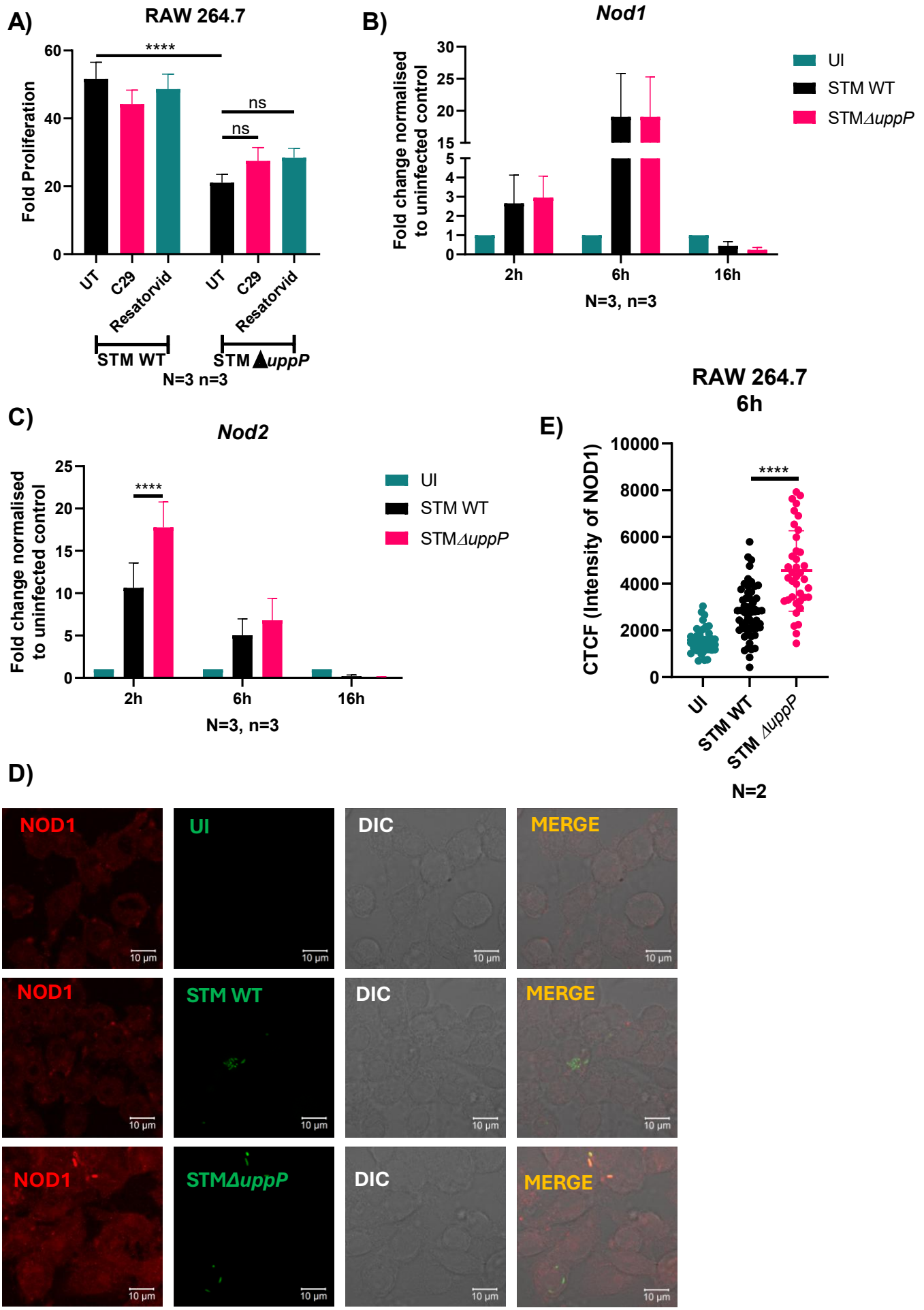
A)
RAW 264.7
Fold Proliferation
60
40
20
0
****
ns
ns
UT
C29
Resatorvid
UT
C29
Resatorvid
STM WT
STM ΔuppP
N=3 n=3
B)
Nod1
Fold change normalised to uninfected control
30
25
20
15
5
4
3
2
1
0
2h
6h
16h
N=3, n=3
UI
STM WT
STMΔuppP
C)
Nod2
Fold change normalised to uninfected control
25
20
15
10
5
0
****
2h
6h
16h
N=3, n=3
UI
STM WT
STMΔuppP
E)
RAW 264.7
6h
CTCF (Intensity of NOD1)
10000
8000
6000
4000
2000
0
****
UI
STM WT
STM ΔuppP
N=2
D)
NOD1
UI
DIC
MERGE
NOD1
STM WT
DIC
MERGE
NOD1
STMΔuppP
DIC
MERGE
10 µm